

An investigation of the effect of initial design choices in density-based topology optimization

J.K. van Schoubroeck

Master of Science Thesis

An investigation of the effect of initial design choices in density-based topology optimization

MASTER OF SCIENCE THESIS

For the degree of Master of Science in Precision and Microsystems
Engineering at Delft University of Technology

J.K. van Schoubroeck

July 6, 2017

Faculty of Mechanical, Maritime and Materials Engineering (3mE) · Delft University of
Technology



DELFT UNIVERSITY OF TECHNOLOGY
DEPARTMENT OF
STRUCTURAL OPTIMIZATION AND MECHANICS (SOM)

The undersigned hereby certify that they have read and recommend to the Faculty of
Mechanical, Maritime and Materials Engineering (3mE) for acceptance a thesis
entitled

AN INVESTIGATION OF THE EFFECT OF INITIAL DESIGN CHOICES IN
DENSITY-BASED TOPOLOGY OPTIMIZATION

by

J.K. VAN SCHOUBROECK

in partial fulfillment of the requirements for the degree of
MASTER OF SCIENCE PRECISION AND MICROSYSTEMS ENGINEERING

Dated: July 6, 2017

Supervisor(s):

Dr.ir. M. Langelaar

ir. D.K. Gupta

Reader(s):

Dr.ir. J. Wu

Dr.ir. J.F.L. Goosen

Abstract

In density based topology optimization, the initial design is an important parameter. The commonly used homogeneous density distribution is generally applicable and does not require computation. However, problem specific initial designs exist that improve the quality of the final result, the required computational cost, or both. Using these two measures, three initial design types are compared with this homogeneous distribution using three optimizers. These are the commonly used Optimality Criteria, Method of Moving Asymptotes and generally well performing algorithm IPOPT. The robustness of these optimizers to poorly performing initial designs is also investigated. The comparison is performed using a rigorous analysis method which involves optimizing a large, diverse, set of benchmark problems and analyzing the results using performance profiles. The first initial design, based on Constructal Theory, performs poorly independent of the optimizer used. The second initial design, the approximate solution to the unpenalized problem, results in better designs at similar computational cost when using IPOPT. The optimizers OC and MMA only benefit from this initial design for some problem types. MMA converges to KKT points in less than 10% of the problems and the initial designs did not improve this. Regarding robustness, IPOPT performs well, resulting in designs of comparable performance to the homogeneous density distribution. The performance of OC severely deteriorates.

Table of Contents

Abstract	i
Acknowledgements	v
1 Introduction	1
1-1 Research purpose and thesis outline	2
1-2 Why are topology optimization problems difficult?	3
1-2-1 General problem definition	3
1-2-2 Local minima due to the SIMP approach	4
2 Topology optimization problems	8
2-1 The problem library	8
2-1-1 Minimum compliance problems	8
2-1-2 Minimum volume problems	10
2-1-3 Compliant mechanism design problems	11
2-2 SIMP parameters and density filter	12
3 Optimizers and settings	13
3-1 Optimizers	13
3-2 Termination criteria	14
4 Initial design types	15
4-1 Homogeneous density distribution	15
4-1-1 Theory	15
4-1-2 Method	15
4-1-3 Application	15
4-2 Constructal Theory	16

4-2-1	Theory	16
4-2-2	Method	17
4-2-3	Application	18
4-3	Solution to the unpenalized problem	18
4-3-1	Theory	19
4-3-2	Method	19
4-3-3	Application	20
4-4	Generation of poorly performing design	21
4-4-1	Theory	21
4-4-2	Method	21
4-4-3	Application	22
5	Comparison method	23
5-1	Performance profiles	24
5-2	Performance profiling of initial design influence	24
5-3	Penalization of inaccurate designs	26
5-4	Limitations	26
5-5	A versatile method to generate performance profiles	26
5-5-1	Application example	27
6	Numerical experiments results for initial designs	30
6-1	Minimum compliance problems	30
6-2	Minimum thermodynamic compliance problems	31
6-3	Compliant mechanism design	32
6-4	Initial design performance discussion and conclusion	33
7	Numerical experiments results for optimizer robustness	35
7-1	Minimum compliance problems	35
7-2	Compliant mechanism design	36
7-3	Optimizer performance discussion and conclusion	37
8	Discussion	39
8-1	On when performance curves differ significantly	39
8-2	Learning from the data	40
9	Conclusion and future work	43
A	Difficulties in Topology Optimization: mathematical background	45
A-1	Computational complexity theory	45
A-2	Convexity: to be or not to be	46

B	Constructal Theory details	48
B-1	The original CT	48
B-1-1	Zeroth order element	48
B-1-2	First order element	50
B-1-3	Second order element	51
B-2	Remarks and adjustments	52
B-2-1	Adjustments to constructs	52
B-2-2	Closing remarks	53
C	Constructal Theory derivations	54
C-1	Derivations of the original Constructal Theory	54
C-1-1	Heat flow in zeroth order construct	54
C-1-2	Optimizing the zeroth order construct	56
C-1-3	First order construct	57
C-2	Derivations of modified Constructal Theory	58
C-2-1	First order construct	58
D	Area to point flow through the dislodging of elements	61
E	Problem library performance profiles	64
F	Computational cost of different mesh sizes	72

Acknowledgements

The Dutch saying

“Een goed begin is het halve werk”

states that if you are off to a good start you have already realized half of your ambitions. Although I hope to raise your interest in finding such starting point in the rest of this document, the reason I mention this is to indicate the luck I had working under the supervision of Deepak and Matthijs. From the first day on they granted me full confidence regarding my research ideas. I chose to perform my thesis at the university because I wanted to experience academic research and improve my writing. Deepak and Matthijs their supervision fully supported this, them both having a deep understanding of the problems at hand and an amazing knowledge of the English language. Our meetings were productive, full of humor, and I always left with enthusiasm and energy. Deepak, Matthijs, thank you for this joyful collaboration.

My appreciation also goes out to Susana and Matthias from the Technical University of Denmark, with whom I had several interesting and fruitful discussions.

I would like to thank Thijs, with whom I have now shared eight years of engineering studies and enthusiasm for the fascinating developments around us. I am sure this is not the last of our studies together. I am thankful to Michiel and Bas who are always in for an in depth discussion on physics or the reviewing of some code. Carmen and Tessa, I am grateful for your encouragement and for being critical about my ambitions. There is still so much you can teach me.

Finally, I want to thank my mother, Paula Kleinheerenbrink, and father, Frank van Schoubroeck, for their support, belief and advice during all of my studies. It is you to whom I would like to dedicate this work.

Nomenclature

Abbreviations

CT	Constructal Theory
FE	Finite Elements
HOM	Homogeneous density distribution, commonly used initial design.
ID	Initial design
IPOPT	Interior point optimizer.
KKT conditions	Karush - Kuhn -Tucker conditions, necessary first-order conditions for a design point to be a local minimum
MMA	Method of Moving Asymptotes, type of optimizer.
OC	Optimality Criteria, type of optimizer.
SIMP	Simplified Isotropic Material with Penalization, material interpolation method.
TO	Topology Optimization
UP	Unpenalized problem
VTPF	Volume-to-point flow problem.

Chapter 1

Introduction

Topology optimization (TO) is a computational method that optimizes the distribution of material in a design domain in order to maximize the performance of the system under specified loading conditions (Bendsøe and Kikuchi, 1988). Although initially developed for load carrying structures, the mathematical framework of TO enables its application to a variety of material distribution problems. An example is the design of a microfluidic mixer (Andreasen et al., 2009) with the aim of maximizing the mixing of two fluids with different temperature. The design domain is a rectangular pipe with specified length where a constraint defines the maximum pressure drop. Although well performing designs are obtained in multiple case studies, reported computation times are 92 and 165 hours. TO has also been applied to multi-physics problems such as the design of an electrothermomechanical actuator (Sigmund, 2001a,b). Here, the application of a voltage across the domain causes heating, deforming the structure in such a way that it can be used as an actuator.

Conventional TO formulations discretize the design domain into several finite elements (FE). A distribution of material consists of solid and void elements and this element-wise presence of material is taken as the optimization problem variables (Bensøe and Sigmund, 2003). The finer the discretization of the design domain, the more complex the possible topologies can be.

It is difficult to solve this type of discrete optimization problem due to the large number of design variables and multiple constraints (e.g. Beckers (1999)). Instead, continuous variables, representing the material density inside each element, and gradient based optimizers are used. Although these converge quickly, they are prone to terminate in local minima which exist due to the penalization of intermediate density elements (Sigmund and Petersson, 1998; Verbart et al., 2011; van Dijk et al., 2010) and some problem physics (e.g. Lau et al. (2001)). Furthermore, optimizing problems within practical computations times prohibits global searches in the typically large design space. Thus, in density based TO, the starting point of the local search has a major influence on the final result (Sigmund and Petersson, 1998; Rozvany, 2009). In this research, we systematically investigate the relation between initial design (ID) choices and the effects these have on the quality of the final result and the required computation time.

The current TO method can be seen as a two step process. The first step consists of choosing a starting point, represented by an initial design. In the second step a gradient-based optimizer uses this point to converge to a nearby solid-void solution. Ideally, the first step yields an initial design that places the optimizer at a point that enables it to converge to the global minimum. This requires knowledge about that minimum's precise position, which cannot be computed for anything but small problem sizes (e.g. Stolpe and Svanberg (2003), Tovar and Khandelwal (2011)). Currently, a homogeneous density distribution (HOM), not requiring any computation, is commonly used for almost all density based TO problems. However, more problem specific initial designs are worth investigating due to these likely resulting in higher quality final results, reduced computation times, or both.

To the best of our knowledge, a detailed study on possible initial design choices and their effects has not been performed. Sigmund and Maute (2013) investigate the effect of starting with a solid-void design. Using that initial design, only slight, slowly occurring, modifications are performed by the optimizer. Lohan et al. (2015) generate an initial design for SIMP using an evolutionary approach. This initial design outperforms HOM, proving better initial designs exist, but the associated large increase in computational cost makes it unpractical. In this paper we investigate initial designs that potentially improve the final objective function value while maintaining competitiveness with HOM regarding the total computation time.

Initial design generation methods can be split in two general classes. The first is methods that optimize a material layout for a specific physics application, which structure may contain valuable information. Examples are Constructal Theory (Bejan, 1997) and The Erosion Model (Errera and Bejan, 1998). The first produces dendritic structures for heat and mass transfer problems by tiling slender elements. The second mimics erosion in river drainage basins by removing material that experience large pressure drops. The second method consists of generally applicable mathematical methods. A few examples follow. In a global search all possible options are evaluated (e.g. Christian et al. (2016)). This can be done in a stochastic fashion using, for example, Monte-Carlo methods (Wenzel and Hamacher, 1999). Alternatively the global optimum can be found using deterministic methods such as branch-and-bound algorithms (Horst and Tuy, 1995). Evolutionary methods mimic the biological process of evolution by selecting, mutating, and combining different designs according to a fitness function (Bäck, 1996) but generally perform poorly for TO problems (Sigmund, 2011). In fractal-based optimization methods (e.g. Salimi (2015)) search directions and step sizes are chosen using fractals, geometrically represented as structures that contain overlaying copies of themselves. Thus, although many alternative methods to generate initial designs exist, the value of these designs for TO, has not been investigated.

1-1 Research purpose and thesis outline

The purpose of this thesis is to systematically investigate the effect of the use of three different initial design generation methods on the performance of a large test set of TO problems (Rojas-Labanda and Stolpe, 2015a) using the SIMP formulation. The chosen methods are all deterministic in order to guarantee reproducibility of the results. The first method, chosen for its low computation cost and ease of implementation, is Constructal Theory (CT) (Bejan, 1997). The second is an approximate solution to the unpenalized TO problem (UP) (Tovar

and Khandelwal, 2010). Finally, an explicitly chosen poorly performing design is generated in order to examine the optimizer robustness.

Due to the final result being dependent on the optimizer chosen, each initial designs generation method is evaluated using three different optimization algorithms. The first and second are, the in the community well-established, Optimality Criteria (OC) (Rozvany and Zhou, 1991; Zhou and Rozvany, 1991) and the Method of Moving Asymptotes (MMA) (Svanberg, 1987). The third is the in TO generally well performing (Rojas-Labanda and Stolpe, 2015a) interior point method IPOPT (Wächter and Biegler, 2006). The performance of the initial-design optimizer combinations is evaluated using a rigorous analysis method. This consists of first optimizing a large test set of standard TO problems using each combination, followed by the comparison of these results using performance profiles (Dolan and Moré, 2002). Using these profiles, both a global indication of, and a ratio between the performance of the methods can be obtained.

All in all, the main research question of this thesis is:

Is there an initial design generation method that can compete with the homogeneous density distribution regarding the final objective function value and total required computational cost?

This question is subdivided into the following questions:

1. What types of methods exist to generate initial designs?
2. How can the performance of initial designs be compared?
3. Is the performance of an initial design optimizer dependent?
4. How do optimizers handle explicitly chosen poorly performing initial designs?

This thesis is built up as following. The remainder of this chapter further describes why TO problems are difficult. Chapter 2 contains the set of benchmark problems, followed by a description of the used optimizers and stopping criteria in Chapter 3. In Chapter 4 the investigated initial design types are described. The comparison method can be found in Chapter 5. The results of the numerical experiments concerning the initial design types can be found in Chapter 6 while the optimizer results are contained in Chapter 7. Finally, a conclusion and an outlook for possible future work can be found in chapter 9.

1-2 Why are topology optimization problems difficult?

The remainder of this chapter describes why TO problems are difficult. First the general TO problem is formulated as a nonlinear optimization problem., followed by a description of how local minima are introduced by the SIMP approach.

1-2-1 General problem definition

In the most general sense, topology optimization aims to answer the question: what material distribution minimizes an objective function F while possibly subject to M constraints $G_i \leq 0$,

$i = 1 \dots M$. For every point in the design domain, $\mathbf{x} \in \Omega$, the material density is indicated by the density variable $\rho(\mathbf{x})$. The naturally discrete problem is relaxed in order to enable practical computation using a large number of variables and constraints. The TO problem is defined in the general optimization problem formulation as

$$\begin{aligned} \underset{\rho}{\text{minimize}} \quad & F = F(\mathbf{u}(\rho), \rho) = \int_{\Omega} f(\mathbf{u}(\rho), \rho) dV, \\ \text{subject to:} \quad & G_i(\mathbf{u}(\rho), \rho) \leq 0, j = 1, \dots, M, \\ & 0 \leq \rho(\mathbf{x}) \leq 1, \forall \mathbf{x} \in \Omega. \end{aligned} \tag{1-1}$$

Here the state field \mathbf{u} satisfies a state equation (Sigmund and Maute, 2013).

Before continuing with the origins of local minima let us discuss why this approach is at all necessary. Why can we not perform a global search of the design space in order to localize the global minimum? Or why can we not start from a large number of evenly spaced different initial designs, followed by a selection of the best final result? Both these approaches are based on the principle that the more possibilities analyzed, the higher the probability of finding the global minimum. Although this is true, the design space of TO problems is simply too large to even analyze a fraction of possible material distributions.

In order to emphasize this, consider a small-sized TO problem with a 1000 finite elements of equal volume and a volume fraction of 0.25. There are a total of $P(1000, 250) \approx 10^{735}$ possible combinations of distributing the 250 solid elements. Many of these combinations can be ruled out using two assumptions. Firstly, that all material should be present in order to reach optimality (active volume constraint) (Stolpe, 2010). Secondly that the location of 10% of the solid material is known due to the problem physics. This results in a problem with 225 solid elements that can be placed in 975 possible locations, resulting in $\binom{975}{225} \approx 10^{227}$ possible combinations. Although greatly reduced, analyzing even a fraction of the combinations is computationally impossible in a practical amount of time for anything but the smallest problem sizes (e.g. Rasmussen and Stolpe (2008)). For that reason, this study is focused on the generation of a single initial design, and the use of that in one optimization run.

1-2-2 Local minima due to the SIMP approach

By optimizing the continuous TO formulation, as described by definition 1-1, using gradient based optimizers enables the use of a large number of variables with multiple constraints. The material properties of the intermediate densities are obtained through an interpolation scheme. The most commonly used scheme is Simplified Isotropic Material with Penalization, or SIMP (Bendsøe, 1989). In SIMP, the relation between the density and the modulus of elasticity of an element i is

$$E_i(\rho) = E_{\min} + \rho_i^p (E_{\max} - E_{\min}). \tag{1-2}$$

Note the penalization parameter p and the minimum value of E_{\min} , included in order to prevent the global stiffness matrix \mathbf{K} becoming singular. Figure 1-1 indicates how the penalization parameter changes the relation between the density and stiffness. When $p = 1$ a linear relation exists between the density and stiffness. When $p > 1$ intermediate density elements

have a low stiffness in comparison to their volume (the cost). As these are unfavorable, the optimizer converges to designs with little intermediate density elements. Unfortunately, local minima are introduced in the solution topography when $p > 1$.

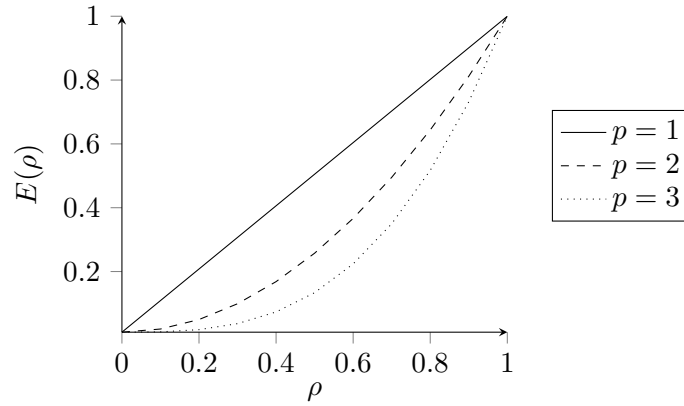


Figure 1-1: Relation between the modulus of elasticity and the penalization parameter.

An illustrative example

In this section, a simple example is used to visualize how non-convexities arise due to the application of penalization. It consists of a minimum compliance optimization problem. Consider two parallel springs k_1 and k_2 as visible in Figure 1-2. Both springs are rigidly attached on the left hand side. Furthermore they are connected through a rigid beam on the right hand side. On the middle of the beam a static force \mathbf{f} is exerted with a magnitude of f in the right direction.

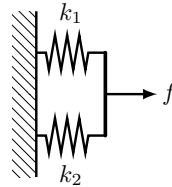


Figure 1-2: Setup of optimization problem: what distribution of material between spring k_1 and k_2 minimizes the displacement of the vertical bar when under a constant load f ?

The objective of this optimization problem is minimizing the displacement of the right spring tips, denoted by u_2 , under the load \mathbf{f} . The densities, ρ , of the springs are the problem variables. The springs are naturally either present, with a density of one, or absent, with a density of zero. In this example, the densities are taken as continuous variables, with $0 \leq \rho \leq 1$, in order to demonstrate how non-convexities arise in the SIMP formulation. The optimization problem is written as

$$\begin{aligned}
 & \underset{\rho}{\text{minimize}} && F = F(\mathbf{u}(\rho), \rho) \\
 & \text{subject to:} && \rho_1 + \rho_2 \leq 1, \\
 & && \mathbf{K}\mathbf{u} = \mathbf{f} \\
 & && 0 \leq \rho_i \leq 1, i = 1, 2.
 \end{aligned} \tag{1-3}$$

Where $\mathbf{K}\mathbf{u} = \mathbf{f}$ is the equilibrium equation that is to be met. In order to satisfy the volume constraint one spring may be solid. A derivation of the objective function follows. Each spring has a stiffness matrix equal to

$$K_{\text{spring}} = k(\rho) \begin{bmatrix} 1 & -1 \\ -1 & 1 \end{bmatrix}. \quad (1-4)$$

Assembling the stiffness matrix to complete the equations of motion yields

$$(k_1(\rho_1) + k_2(\rho_2)) \begin{bmatrix} 1 & -1 \\ -1 & 1 \end{bmatrix} \begin{bmatrix} u_1 \\ u_2 \end{bmatrix} = \begin{bmatrix} 0 \\ f \end{bmatrix}. \quad (1-5)$$

Now solving for u_2 yields the displacement on the right node as $u_2 = f/(k_1(\rho_1) + k_2(\rho_2))$. For the remaining part of this example f will be considered constant and the aim is to minimize the objective function $u_2 = 1/(k_1(\rho_1) + k_2(\rho_2))$. Finally, applying the SIMP formulation in the relation between the spring density and stiffness yields the objective function as

$$u_2(\boldsymbol{\rho}) = \frac{1}{\rho_1^p k_1 + \rho_2^p k_2}. \quad (1-6)$$

In order to calculate this displacement spring stiffnesses are chosen as $k_1 = 0.8$, $k_2 = 1$.

Let us consider the problem before applying penalization, thus with $p = 1$. Minimum compliance problems are convex due to the more material present in the springs, the stiffer they are thus the lower the objective function (Pettersson, 1999). In this problem, the volume constraint is active at optimality.

The value of the objective function for $p = 1$ can be seen in Figure 1-3 with the material allocated to k_1 on the horizontal axis and the objective function value on the vertical axis. The solid line is convex and indicates a minimum in the objective function value when all material is present in the second spring, as expected. Furthermore, a gradient based optimizer converges to this minimum whatever the initial density distribution.

Next consider the curve of the objective function for $p = 1.5$. The penalization parameter causes the solution topography to contain two different local minima. For different initial density distributions, different minima will be found by a gradient based optimizer. The curve for $p = 2$ demonstrates how a higher value of p assists in converging to a binary design.

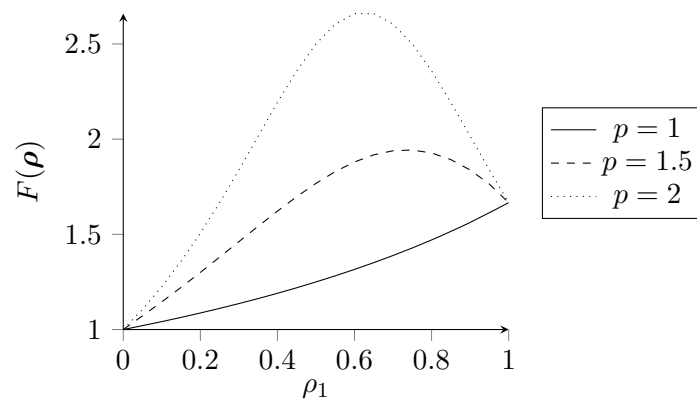


Figure 1-3: Objective function value for the two-spring example under different penalization values.

Topology optimization problems

This chapter contains the set of test problems used to investigate the performance of certain optimizer initial design combinations. In general, the validity of the observations deduced from these experiments depend on the set of test problems. They must properly represent every TO problem the optimizer ID combinations are expected to optimize. It is for this reason that the test set of problems as described by Rojas-Labanda and Stolpe (2015a) is used. It contains a large number of structural TO benchmark problems of varying difficulty, lying in three different problem classes. These are minimum compliance, minimum volume, and compliant mechanism design. Each class contains multiple problem types, defined by the boundary conditions and design domain. Furthermore, each problem type is tested using different parameters in order to obtain a large set of problems.

2-1 The problem library

The first two columns of Table 2-1 indicate the problem library. The three problem classes are shown in the first column, followed by the problem types contained in each class. In addition to the original library used by Rojas-Labanda and Stolpe (2015a) one problem type is added in order to enable the investigation of Constructal Theory as an initial design. This problem consists of minimizing the thermodynamic compliance of a heated plate (Bensøe and Sigmund, 2003). Sections 2-1-1 to 2-1-3 describe the problem types, design domain aspect ratios, finite elements per unit length and constraints per problem class. All of the problems are two dimensional.

2-1-1 Minimum compliance problems

In this problem class the objective is to minimize the compliance under a volume constraint. The dictating equilibrium equation is found by applying the finite element method to the dictating partial differential equation and is $\mathbf{K}(\mathbf{t})\mathbf{u} = \mathbf{f}$. Here $\mathbf{u} \in \mathbb{R}^d$ indicates the nodal displacements, $\mathbf{t} \in \mathbb{R}^n$ the element wise densities, and $\mathbf{f} \in \mathbb{R}^d$ the external load. The total

Table 2-1: The problem library consists of the three problem classes, contained in the first column, and contained problem types, indicated by the second column. Not all IDs and optimizers have been used for every problem. Combinations that are examined are indicated with a tick.

Problem class	Problem type	Initial design				Optimizer		
		CT	HOM	UP	BAD	OC	MMA	IPOPT
Minimum compliance	Heated plate	✓						
	Cantilever		✓	✓	✓	✓	✓	✓
	Michell truss	✗						
	MBB beam							
Minimum volume	Heated plate	✓						
	Cantilever		✓	✓	✓	✗	✓	✓
	Michell truss	✗						
	MBB beam							
Compliant mechanism design	Inverter							
	Gripper							
	Amplifier	✗	✓	✓	✓	✓	✓	✓
	Lever							
	Crimper							

number of degrees of freedom is indicated by d and n indicates the number of finite elements. The stiffness matrix \mathbf{K} , with size $\mathbb{R}^n \rightarrow \mathbb{R}^{d \times d}$, is well conditioned through the application of a small, positive density for elements with a density of zero (see the SIMP formulation in Section 1-2-2). The problem is formulated as

$$\begin{aligned}
 & \underset{\mathbf{t}}{\text{minimize}} && \mathbf{u}^T(\mathbf{t})\mathbf{K}(\mathbf{t})\mathbf{u}(\mathbf{t}), \\
 & \text{subject to:} && \mathbf{a}^T \mathbf{t} \leq V, \\
 & && \mathbf{0} \leq \mathbf{t} \leq \mathbf{1}.
 \end{aligned} \tag{2-1}$$

Here \mathbf{a} indicates the relative volume of the elements. This formulation contains a nonlinear objective function with linear inequality constraints. The volume fraction lies between zero and one: $0 < V \leq 1$ (Rojas-Labanda and Stolpe, 2015a).

For the test set of minimum compliance problems, two types of physics are considered. The first is mechanical compliance. Here the standard TO problems are optimized, consisting of the Michell truss, the Cantilever, and the MBB beam. The boundary conditions of these problems can be seen in Figure 2-1a to 2-1c. The second type of physics considered is the thermodynamic compliance Bendsøe and Sigmund (2003). In this problem a heat load is incident on a rectangular plate which contains a heat sink on a segment of one edge and adiabatic boundaries around the rest of the domain. The domain of this problem can be seen in Figure 2-1d. In this case the variables \mathbf{u} in problem definition 2-1 indicate the nodal temperatures.

For the mechanical compliance problems five different volume fractions are considered. These range from 0.1 up to 0.5 in steps of 0.1. Furthermore, each problem type is optimized using multiple domain ratios and a different number of elements per unit length as indicated in Table 2-2. There are a total number of 225 unique minimum mechanical compliance problems.

Table 2-2: The test set of the minimum mechanical compliance, minimum mechanical volume and compliant mechanism design problems are defined by different domain ratios [nelx:nely] and number of elements per unit length N_l .

Problem type	Domain aspect ratios	N_l
Michell	1:1, 2:1, 3:1	20, 40, 60, 80, 100
Cantilever	2:1, 4:1	
MBB	1:2, 1:4, 2:1, 4:1	
All compliant mechanisms	1:1, 2:1	

Table 2-3: Details of the test set of minimum thermodynamic compliance problems.

Problem type	Conductivity ratios	Volume fractions
Heated plate	100, 150, ..., 1000	0.1, 0.15, ..., 0.4

The application of Constructal Theory to thermal problems is relatively evident, for this reason it is applied to the problem of minimizing the thermodynamic compliance. When using CT to generate an ID, the variables are the conductivity ratio between the high and low-conductivity material, \tilde{k} , and the volume fraction. The domain aspect ratio and resulting number of FE elements follows from CT (detail in Chapter 4). The minimum number of FE elements is set to 1000, the smallest and largest problem sizes include 6204 and 204440 elements. As shown in Table 2-3, the conductivity ratios considered are from 100 up to and including 1000 in steps of 50. The volume fractions used range from 0.1 up and including 0.4 in steps of 0.05. Using these variables there are a total number of 133 unique minimum thermodynamic compliance problems.

2-1-2 Minimum volume problems

In the minimum volume problems the amount of material in the domain is minimized under a compliance constraint. The problem formulation is similar to the minimum compliance problem but now formulated as

$$\begin{aligned}
 & \underset{\mathbf{t}}{\text{minimize}} && \mathbf{a}^T \mathbf{t}, \\
 & \text{subject to:} && \mathbf{u}^T(\mathbf{t})\mathbf{K}(\mathbf{t})\mathbf{u}(\mathbf{t}) \leq C, \\
 & && \mathbf{0} \leq \mathbf{t} \leq \mathbf{1}.
 \end{aligned} \tag{2-2}$$

Here $C = k(\mathbf{u}^T(\mathbf{t}_0)\mathbf{K}(\mathbf{t}_0)\mathbf{u}(\mathbf{t}_0))$, indicating the compliance must be no more than a factor k larger than the compliance of a homogeneous density distribution \mathbf{t}_0 (Rojas-Labanda and Stolpe, 2015a). This distribution consists of all elements having a density of a half, $\mathbf{t}_0 = 0.5 \cdot \mathbf{1}$.

As in the minimum compliance problems two types of physics are considered: mechanical and thermodynamic compliance. For the mechanical problems, the used domain sizes and discretizations per unit length are equal to the minimum compliance problems and shown in Table 2-2. There are a total number of 135 unique mechanical minimum volume problems. For the thermodynamic compliance the procedure followed is equal to the procedure used in the minimum compliance problems. Considering the number of FE elements, the smallest

Table 2-4: Compliance ratios of the minimum mechanical and thermodynamic volume problems.

Physics application	Compliance ratio k
Mechanical minimum volume	1, 1.2, 1.5
Thermodynamic minimum volume	1, 1.1, ..., 1.5

and largest problem sizes include 5760 and 33572 elements. There are a total number of 114 unique thermodynamic minimum volume problems.

The compliance ratios, k , for the two physics applications can be seen in Table 2-4. For the mechanical problems values of 1, 1.2 and 1.5 are considered. For the thermodynamic minimum volume problems k ranges from 1 up to and including 1.5 in steps of 0.1. This is done in order to maintain a large problem library.

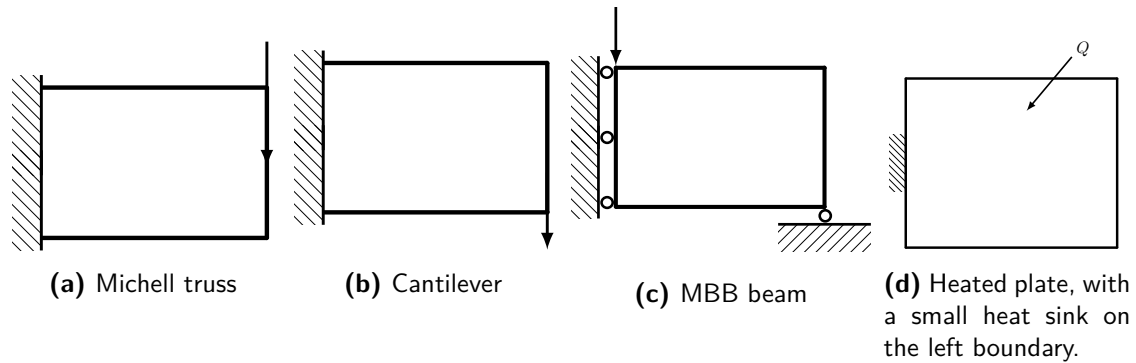


Figure 2-1: Minimum compliance and volume problem designs domains and boundary conditions. For the first three problems, the arrows indicate the application of a force while a uniform heat load is applied on the heated plate.

2-1-3 Compliant mechanism design problems

In compliant mechanism design problems, the aim is to transfer a force applied at the input node u_{in} to an output node u_{out} , subjected to a constraint on the permissible amount of material. The problem formulation is

$$\begin{aligned}
 & \underset{\mathbf{t}}{\text{maximize}} && \mathbf{l}^T \mathbf{u}(\mathbf{t}), \\
 & \text{subject to:} && \mathbf{a}^T \mathbf{t} \leq V, \\
 & && \mathbf{0} \leq \mathbf{t} \leq \mathbf{1}.
 \end{aligned} \tag{2-3}$$

Here \mathbf{l} is a vector with zeros for all degrees of freedom except the one associated with the output degree of freedom (Rojas-Labanda and Stolpe, 2015a). The objective function is nonlinear.

There are five different design problems. These are the force inverter, the gripper, the amplifier, the lever and the crimper. The problem domains and boundary conditions are shown in Figure 2-2. Five different discretizations per unit length are considered for two different domain ratios. These are stated in Table 2-2. The range of the volume fraction is from 0.1 up to and including 0.5 in steps of 0.1.

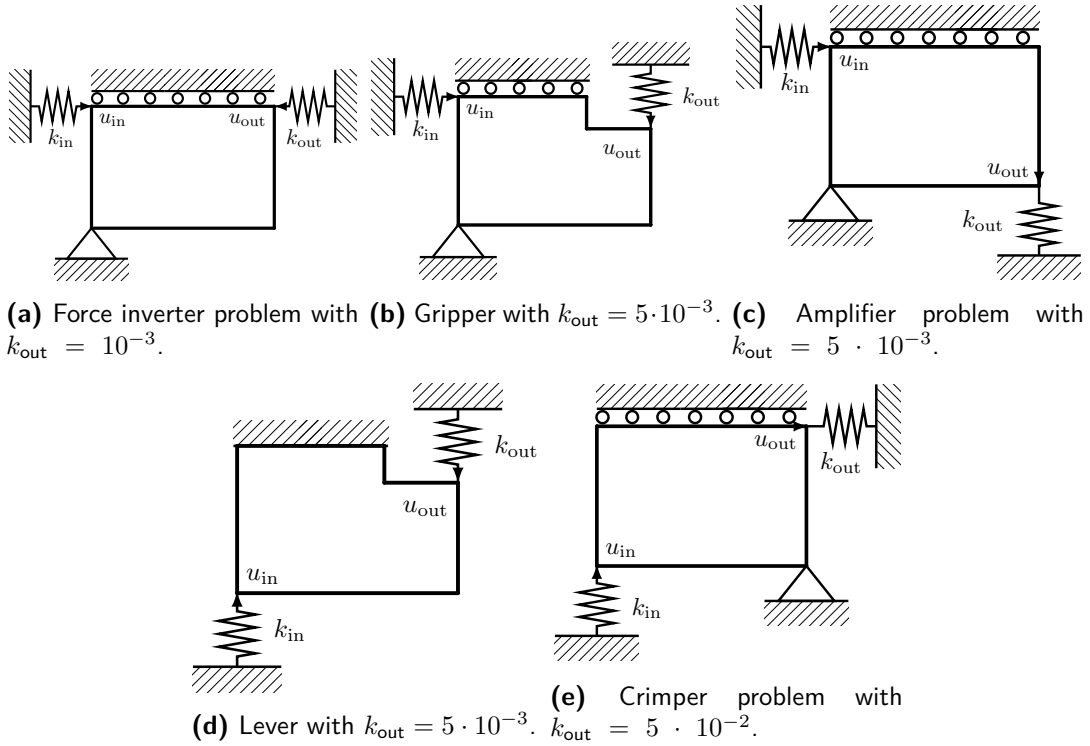


Figure 2-2: Compliant mechanism design domains and boundary conditions. The input spring stiffness, k_{in} , is one for all problems.

2-2 SIMP parameters and density filter

The problem instances are all formulated using the SIMP approach with the standard penalization value of $p = 3$. A Python version of the standard 88-line MATLAB code (Andreassen et al., 2011) is modified to optimize the problems. The modifications are performed in order to be able to optimize the different problem classes using the optimizers. The originally in C++ written optimizer IPOPT is accessed through the open-source Python wrapper *cyipopt*.

In order to prevent checkerboards a density filter is applied (Bourdin, 2001). In this filter, element densities are modified according to a weighted average of the neighboring element densities in a radius r_{min} . The weighted average is defined by $\bar{H}_{e,i} = \max(0, r_{min} - \Delta(e, i))$ where $\Delta(e, i)$ indicates the distance from element e to element i . The modified element density is defined by

$$\tilde{k}_e = \frac{1}{\sum_{i \in N_e} \bar{H}_{e,i}} \sum_{i \in N_e} \bar{H}_{e,i} t_i.$$

Here N_e is the set of elements that lie within a radius of r_{min} of element e . In this research, the filter radius, r_{min} , is constant with respect to the element size and set to a value of 1.2. This results in mesh-dependent topologies that permit smaller feature sizes when increasing the number of finite elements per unit length. In this manner, the amount in which the performance of topologies can differ is also larger for a set discretization; optimizer and initial design configurations have more possibilities of distancing themselves from each other.

Optimizers and settings

The three optimizers used in this paper are Optimality Criteria Rozvany and Zhou (1991); Zhou and Rozvany (1991), the Method of Moving Asymptotes Svanberg (1987), and IPOPT Wächter and Biegler (2006). Many other optimizers can be used for TO problems (for extensive benchmark see work by Rojas-Labanda and Stolpe (2015a)). Examples are Sequential Quadratic Programming (Boggs and Tolle, 1995), the dual optimizer using convex approximations CONLIN (Fleury, 1989) and the globally convergent version of MMA, GCMMA (Svanberg, 2002). However, OC and MMA are the most used optimizers, while IPOPT was found to be generally well performing.

3-1 Optimizers

Optimality Criteria (OC) is a first order optimization procedure that was originally derived by considering the strain energy as an indicator where material should be added and where it should be removed. OC only functions when the derivative of the objective function to the design variables is always negative. It can thus not be used for minimum volume problems. The OC optimizer used in this paper is as stated in the 88-line code of Andreassen et al. (2011). Two modifications have been performed. Firstly, the difference between the estimates of limits of the constraint Lagrange multiplier has been reduced. Secondly, modifications have been made following Bensøe and Sigmund (2003) in order for OC to be able to handle compliant mechanism design problems.

The Method of Moving Asymptotes (MMA) optimizer is a first order method that sequentially generates approximations of the local solution topography. In MMA, this approximation is convex and can be efficiently solved. The found solution to the convex problem is the starting point for the next iteration. MMA modifies the asymptotes that define the approximation every iteration in order to prevent them being too conservative. This prevents a slow convergence.

IPOPT is an interior-point optimizer that has been found to be a well performing independent of the TO problem type Rojas-Labanda and Stolpe (2015a). It is a second-order method that

approximates the second derivative of the objective function to the design variables using a limited-memory BFGS algorithm. IPOPT is the only one of three optimizers where the number of solves is not always equal to the number of iterations. This is due to IPOPT sometimes calling the objective function value multiples times per iteration.

3-2 Termination criteria

It is desirable to stop an optimization run when the used optimizer does not further improve the design. This occurs when an optimizer converges to a local optimum. In what part of this convergence path to stop the optimizer is a sensitive business. Stopping the optimizer when the difference between two consecutive iterations is below a given threshold might interrupt the optimizer prematurely. Furthermore, precise stopping criteria exist in the form of the Karush - Kuhn - Tucker (KKT) conditions. A measure of optimality of a design point is found by taking the Euclidean norm of these conditions. In this paper, an optimizer terminates due to one of two events occurring. The first, and desired event, being the optimizer generating a design that satisfies the Euclidean norm of these conditions within a certain value ω . The second event being the optimizer using the maximum number of solves, set at 1000.

Of the three optimizers used, OC is the only exception. It is stopped when the difference between two designs is below a certain threshold and the design satisfies the constraints. The value ω associated with the finding of a KKT-point is optimizer dependent. Rojas-Labanda and Stolpe (2015a) demonstrated that the amount of designs where MMA finds a KKT-point is highly dependent on the value of ω . On the other hand, IPOPT was able to find designs associated with KKT-points within very small values of ω . For the exact formulation of the KKT-conditions and the associated optimizer dependent values of ω the reader is referred to Rojas-Labanda and Stolpe (2015a).

Initial design types

This chapter contains the theory, method and application of the four tested initial designs. Not all of these are applied to all problems. An overview of all problem types and optimizer and ID combinations is given by Table 2-1.

4-1 Homogeneous density distribution

The homogeneous density distribution (HOM) is currently the community standard initial design for density based topology optimization (Bendsøe and Sigmund, 2003).

4-1-1 Theory

HOM does not contain any problem related information.

4-1-2 Method

The HOM initial design consists of a uniform density field with a value equal to the volume constraint, $\mathbf{t}_{\text{HOM}} = V * \mathbf{1}$. The only exception is minimum volume problems, where the density field has a value of a half, $\mathbf{t}_{\text{HOM, min. vol.}} = 0.5 * \mathbf{1}$.

4-1-3 Application

HOM can be applied to all problems.

4-2 Constructal Theory

Constructal Theory (CT) is used as an inspiration to generate an initial design for the minimum thermodynamic compliance problem. The background theory, generation method, and application to this problem are explained below. Another type of CT inspired initial design generation method, also from Bejan (2001), is also investigated but was not considered due to the high computational cost. For details, the reader is referred to Appendix D.

4-2-1 Theory

CT was developed to unite all types of flow in a single law Bejan (1997, 2001). It aims to prove that geometric form is the mechanism through which a system achieves its objective. The law that forms the basis of CT is the Constructal Law, stated as:

“For a finite-size flow system to persist in time (to live), its configuration must evolve in such a way that it provides easier access to the imposed (global) currents that flow through it.”Bejan (2001)

CT has been applied to a variety of disciplines such as economics, biology, and engineering. Application examples are the optimized cooling of a heat generating volume through natural and forced convection Bejan et al. (1995), volume-to-point heat and fluid flow problems Bejan (1997); Bejan and Errera (1997), predicting the formation of geometrical shapes in fluid systems heated from below (Rayleigh-Bénard convection) Nelson R. A. and Bejan (1998) and the prediction of geometrical shapes in river drainage basins Errera and Bejan (1998).

An approximation of the CT solution to the volume-to-point flow problem (VTPF) Bejan (1997); Bejan and Errera (1997) can be used as an initial design for TO flow problems. CT generates this solution using a large number of steps under multiple assumptions and intermediate optimizations. The aim of the rest of this section is to sketch this process and provide the reader with an idea of the result rather than explain it in detail. For a detailed analysis, discussion of the criticism on CT, and a derivation of the equations the reader is referred to appendix D.

In the VTPF a limited amount of high conductivity material, ϕ , is to be distributed in a finite volume V with the aim of minimizing the maximum occurring temperature due to a heat input $q'''[\text{W}/\text{m}^3]$. This is done by conducting the heat to a sink, present on a small part of the boundary. There is no heat flow across the rest of the boundary. V is described by a width W , length L and height H where $W, L \gg H$. For that reason the optimization is performed in the two dimensional plane LH . The VTPF is similar to the heat conduction TO problem Bendsøe and Sigmund (2003).

The CT solution to the VTPF is dependent on two variables. Firstly the fraction of high conductivity material ϕ . Secondly the conductivity ratio, \tilde{k} , between the high and low-conductivity material. The solution consist of a material distribution and the ratio of the width and length of the domain.

4-2-2 Method

CT generates a solution to the VTPF by assembling *elementary* into *higher order* designs. The extent of this assembly process is dictated by the problem variables ϕ and \tilde{k} .

When $\tilde{k}\phi < 8$ the solution consists of only the elementary design. Here the high-conductivity material is present in the WL plane in the form of a rectangle, running from the heat sink across the domain. An example is visible in Figure 4-1a. The thickness of the blade is dictated by ϕ . The length to width ratio of the domain is optimized in order to minimize the maximum temperature, while keeping the area constant. This ratio is determined by

$$\left(\frac{H_0}{L_0}\right)_{\text{opt}} = \frac{2}{\sqrt{\tilde{k}\phi_{\text{el}}}}. \quad (4-1)$$

Where ϕ_{el} is the volume fraction assigned to the elementary construct, in this case ϕ . For a detailed description of how equation 4-1 is found the reader is referred to appendix B-1-1.

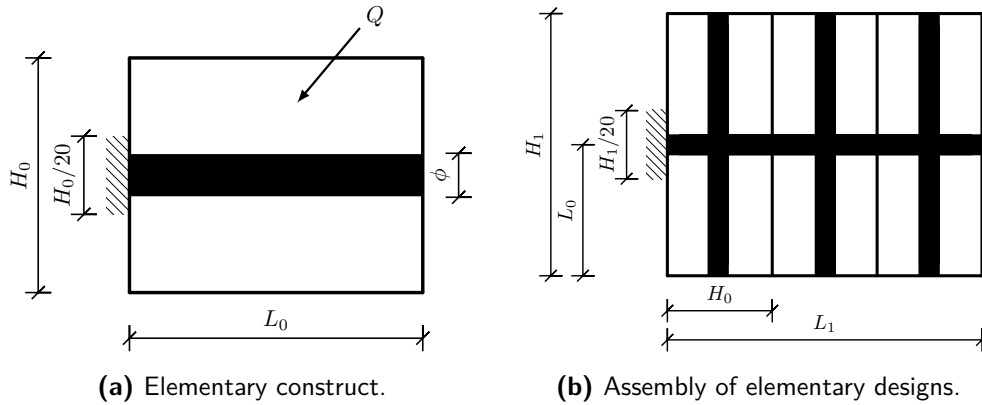


Figure 4-1: CT assembles elementary designs into higher order designs.

When $\tilde{k}\phi \geq 8$, CT assembles multiple elementary designs together to form a more complex material distribution. The elementary tiles are rotated, stacked, and connected to the sink by a central branch. In figure 4-1b six elementary designs are combined in this manner.

In the original CT formulation this assembly process continues by using the new design as a tile and once again rotating and stacking them in order to generate better performing designs. It has however been proven that further assembly decreases the performance (Ghodoossi and Egrican, 2003). Thus an assembly of elementary designs is generated when $\tilde{k}\phi \geq 8$. Considering other additions to CT as suggested by Ghodoossi and Egrican (2003) the remaining assembly dimensions are stated below. For a detailed derivation the reader is referred to appendix C. The elementary design is calculated as in equation 4-1 with the exception that now $\phi_{\text{el}} = \frac{\phi}{2}$, where ϕ equals the problem volume fraction. The optimal number of elementary tiles in the assembly is $n_{1, \text{opt}} = \sqrt{\tilde{k}\phi}$. The maximum temperature is minimized by choosing the aspect ratio as $\left(\frac{H_1}{L_1}\right)_{\text{opt}} = \sqrt{2}$. Finally the thickness of the central branch is dictated by $D_1 = L_0\phi$.

4-2-3 Application

The CT solution to the volume to point flow problem can be used as an ID in TO flow problems and is used in this study for the minimum thermodynamic compliance TO problem Bensøe and Sigmund (2003). Due to CT dictating the domain shape, it has limited applicability. For this study the domain shape is first calculated using CT and the other initial designs are generated using this domain shape.

The use of initial designs in TO requires their description in a discretized design domain. For computational reasons the CT shape is only approximately present in the discretized domain, which is addressed in the next paragraph. The generated ID is thus a CT inspired ID rather than an exact solution as stated by CT. Moreover, in the assembly of elementary designs, the applied material is lower than ϕ . This is due to the elementary and center branch overlapping. This missing material is added as solid elements on both sides of the center branch. For every CTID the volume constraint is always met and the amount of allocated material is never below 95% of the volume fraction.

When optimizing a topology, optimizers such as OC and MMA make only slight modifications per iteration once a design becomes binary. This is due to the optimizers attempting to satisfying the optimality criteria, while the shifting of material causes these to decrease due to the penalization parameter. This effect is known as the *boundary translation problem* (Sigmund and Maute, 2013) and it occurs due to the shifting of a boundary often requiring the escape from a local minima.

The boundary translation problem becomes visible when comparing an initial design with the final design generated using, for example, OC. The more an initial design is represented by elements with a solid density, the more the final result resembles it. In order to fully investigate the value of a CTID, each problem is optimized using a CTID with varying density differences. These indicate the difference in density between the CT shape and the remainder of the design domain. The differences tested are 0.25, 0.5, 0.75, and 1. The occurring density difference is dependent on the mesh size and a maximum deviation of 5% from the exact density difference is tolerated. The smaller this tolerance, the larger the required mesh size. Algorithm 1 indicates how CTID are generated computationally.

4-3 Solution to the unpenalized problem

A commonly used method to minimize the influence of the local minima introduced by the SIMP formulation is the continuation method (Allaire and Kohn, 1993). Here, the penalization parameter is slowly increased with the aim of preventing the early convergence to a poorly performing local minimum. Although convergence to the global optimum is not guaranteed (Stolpe and Svanberg, 2001), the final objective function value is often lower than when using a constant penalization value (Sigmund and Maute, 2013). The unpenalized (UP) initial design can be seen as a continuation method with a single step step in the penalization parameter.

Algorithm 1 Generate CTID

```

1:  $nr_{\text{elem}} \leftarrow 5000$ 
2:  $\phi_{\text{el}} \leftarrow \phi$ 
3: if  $\tilde{k}\phi > 8$  then
4:    $\phi_{\text{el}} \leftarrow \frac{\phi}{2}$ 
5: Generate elementary design
6: while  $\delta_{\text{dens}} > \text{tol}_{\text{dens}}$  do
7:    $\left(\frac{L_0}{H_0}\right)_{\text{opt}} \leftarrow \frac{2}{\sqrt{\tilde{k}\phi_{\text{el}}}}$ 
8:   if  $D_0 < 4$  then
9:      $nr_{\text{elem}} \leftarrow nr_{\text{elem}} + 100$ 
10:   $nr_{\text{elem}} \leftarrow nr_{\text{elem}} + 100$ 
11:  update  $D_0, \left(\frac{L_0}{H_0}\right)_{\text{opt}}$ 
12: if  $\tilde{k}\phi > 8$  then
13:   Generate assembly of elementary designs
14:    $n_{1, \text{opt}} \leftarrow \sqrt{\tilde{k}\phi_1}$ 
15:   Assemble elementary designs
16:   if  $\delta_{\text{dens}} > \text{tol}_{\text{dens}}$  then
17:     Add material to center branch
18: Return design

```

4-3-1 Theory

The unpenalized problem is of interest because the associated solution topography follows the general shape of its penalized counterpart, without the penalization-parameter induced local minima. Consider the set of feasible solutions to an unpenalized TO problem, S_{feasible} . This set is a union of the feasible binary and feasible non-binary solution sets

$$S_{\text{feasible}} = S_{\text{feasible, binary}} \cup S_{\text{feasible, non-binary}}.$$

The value of the unpenalized design is clear when considering the fact that the unpenalized minimum compliance and minimum volume TO problems are convex (Pettersson, 1999). There is one and only one optimum which lies in the feasible solution set, S_{feasible} . Now, the structure of the binary and non-binary solution sets indicate that a binary solution of equal quality does not exist. The solution to the unpenalized problem is a lower bound to the objective function value of the penalized problem. Considering the function of optimization algorithms being the generation of a binary design from a non-binary ID, the global optimum of the unpenalized TO problem is an ID worthwhile investigating.

4-3-2 Method

The unpenalized ID is generated by setting the penalization parameter as $p = 1$ and optimizing the TO problem. The computational expense of TO problems is related to the time required to solve the system of linear equations in the finite element method. The size of the system is dependent on the mesh size of the TO problem. Because one of the performance

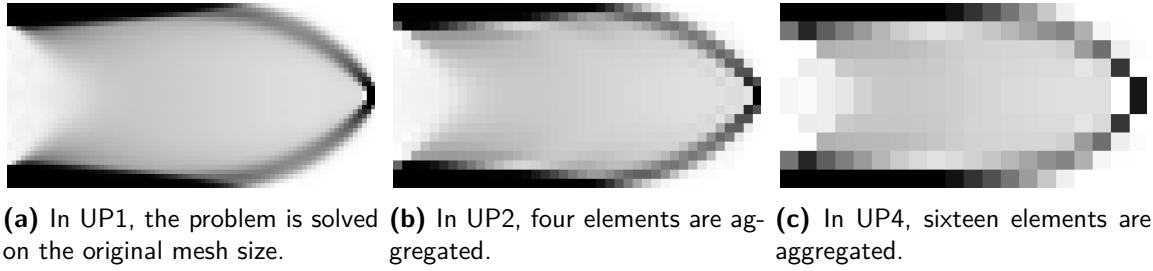


Figure 4-2: Examples of approximate solutions to the unpenalized version of the minimum compliance problem using different mesh sizes. In this case, the problem type is the Michell cantilever, the domain ratio is 2:1 and the maximum volume fraction is 0.3.

indicators of an initial design is the computation expense, three mesh sizes, with a different amount of elements, are used to generate the UP. An example of these mesh sizes is shown in Figure 4-2. The first is a mesh equal to the original mesh and requires the same amount of computation time per solve. The second is a mesh where two elements are combined per axis. In a two dimensional problems of the used test set this results in new square elements that contain four elements of the original mesh, see Figure 4-2b for an example. The third mesh combines four elements per axis. This mesh contains large square elements that contain sixteen of the original mesh finite elements, see Figure 4-2c for an example. In order to assess the computational burden of the two coarse meshes an experiment is performed. The details can be found in Appendix F. The results of this experiment indicate that the required computation time is proportional to the size of the stiffness matrix, and the computational cost of UP are scaled accordingly.

In this thesis the focus lies on the performance of different IDs considering specific optimizers. For that reason, for a specific problem, all optimizers are initiated with the same UPID. This is done by optimizing the unpenalized problem using the same optimizer, namely IPOPT. If instead each optimizer would independently generate the UPID it would be more difficult to distinguish the change of performance due to the quality of the ID from the change of performance due to the quality of the optimizer.

The termination criteria are the same as the original problem except the maximum number of iterations. For minimum compliance and minimum volume problems it is set to 30, whilst for compliant mechanism design problems it is set to 60. Due to the optimizer not always finding a KKT point before the maximum number of iterations is reached, the unpenalized initial design is formally an approximate solution to the unpenalized problem. UP is generated using HOM as an initial design (for details, see Section 4-1).

4-3-3 Application

UPID is applicable to all the test set problems. Furthermore, it can be generated for all problems that are formulated using SIMP.

4-4 Generation of poorly performing design

The previously explained initial design generation methods aim to generate initial designs with a high performance. The poorly performing, or BAD, ID explained in this section, does the opposite. It is generated to have a poor performance. Using these initial designs, the capability of optimizers to handle bad initial designs is researched.

4-4-1 Theory

TO can be considered a two step procedure. First, a starting point is selected. Subsequently a design is generated using that starting point. The performance of the final design can be improved by improving either one of these steps. Moreover, the contributions of both steps are closely related. A well performing initial design using a poorly performing optimizer can yield the same quality final design as a poor initial design optimized by a well performing optimizer. Consider a poorly performing design \mathbf{t}_{bad} . Slight modifications of this design, $\tilde{\mathbf{t}}_{\text{bad}}$, are likely to also perform poorly. The same holds for a well performing design, although the objective function is sensitive to particular sections, random slight modifications still yield a well performing design. The capability of an optimizer to transform a poorly performing design into well function one indicates the capability to traverse a large distance in the design space, thus being resistant to being caught in local minima. If an optimizer demonstrates this type of robustness, it is useful for problems where it is difficult to generate well performing initial designs.

4-4-2 Method

In this research, the bad initial designs are generated by transforming the minimization problem into a maximization problem for minimum compliance and minimum volume problems, and visa versa for compliant mechanism design problems. This is done by multiplying the objective function value and the sensitivities by -1. Furthermore, the constraints are modified in order to obtain a design that is feasible in the original problem statement. An example of two BAD initial designs can be seen in Figure 4-3.

An explanation of the problem dependent BAD initial design generation method follows. For minimum compliance the problems are formulated as maximum compliance problems. The upper bound on the volume is modified to an equality constraint, in order to prevent the optimizer from removing all material. The resulting initial designs often contain little material around the attachment point of the loads and fixed boundary conditions. Figure 4-3a is an example of a BAD initial design for the Michell problem. For minimum volume problems the BAD initial design is a completely solid design domain described by $\mathbf{x}_{0 \text{ BAD, min vol}} = \mathbf{1}$. For compliant mechanisms, the BAD initial design is also generated by multiplying the objective and sensitivities by -1. The resulting mechanism minimize the displacement in the required direction, instead of maximizing it. This results in displacements at the output spring location that are in the direction opposite to the desired one. Figure 4-3b is an example of a BAD initial design for the compliance inverter, the current mechanism displaces the output node upwards instead of downwards.

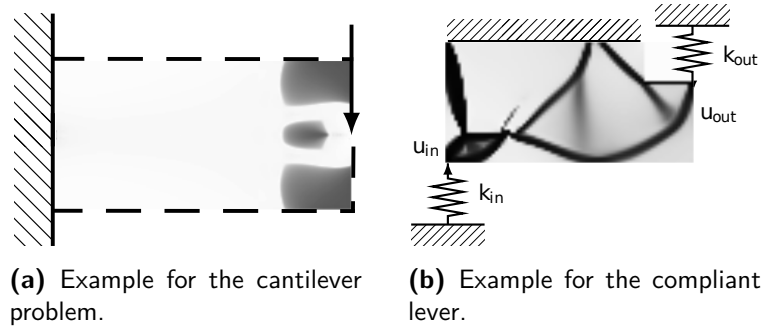


Figure 4-3: Examples of BAD initial designs.

The BAD initial designs are generated using the IPOPT algorithm. For compliant mechanism design problems, the maximum number of iterations is 90. For the remaining problems it is 30. Furthermore, the termination criteria are as for the original optimization problem.

4-4-3 Application

The BAD ID can be applied to all benchmark problems.

Chapter 5

Comparison method

In topology optimization, there are two key performance measures. The first is the quality of the final design and the second is the computational cost of generating it. In this thesis, different initial design and optimizer combinations are compared. These combinations will from now on be addressed as *methods*. The comparison of methods is performed by optimizing a large set of TO problems with each method and comparing the performance measures using *performance profiles* Dolan and Moré (2002).

A comparison of methods is generally performed in order to obtain a global indication of the relative performance of a method, rather than relative capability of a method to solve a particular problem. For that reason the performance measures of methods are often compared using a test set of problems. Naturally, the validity of this comparison improves as the test set of problems better represents any problem the method is expected to solve. With this in mind, test sets are often large and contain problems with different levels of difficulty.

As the difficulty of problems in a test set varies, so will the performance measures of a particular method. Evaluating the performance of a method using these measures is not straightforward. For example, comparing methods using an average or sum of a measure can be misleading, as these values can be dominated by a small subset of problems. Another reason why the comparison of performance measures is difficult is due to the incapability of methods to always produce a result that respects problem specific criteria. When this occurs, there are a few common approaches. One is simply removing the problem from the test set, another is penalizing failing methods. One could also compare methods according to the number of times a feasible design is found, rather than the performance measure. Each approach has a drawback. Removing problems causes information regarding the robustness of methods to be lost while the application of a penalization factor is subjective. Furthermore, counting the number of feasible designs rather than using the actual performance measure values causes information regarding the relative performance to be lost. These difficulties are overcome by using performance profiles.

5-1 Performance profiles

Performance profiles Dolan and Moré (2002) enable the comparison of a single performance measure value of n optimization methods s_1, s_2, \dots, s_n when optimizing m problems p_1, p_2, \dots, p_m . They have been extensively used to compare optimization methods (e.g. Benson et al. (2003)).

Consider the first problem p_1 contained in the problem set P being optimized by every optimization method, s_i with $i = 1, \dots, n$, in the methods set S . Every method s_i may obtain different performance measure values for problem p_1 . Often so, the value of one method will be the minimum value. The values of the remaining methods are each a factor larger than this minimum value. Thus, for problem $p_1 \in P$ we have identified two items. Firstly, the method with the minimum in performance measure value. Secondly, the ratios of the performance measure values of the remaining methods in comparison to this minimum value.

In order to generate a performance profile, the procedure of first solving the problem with each method followed by the calculation of the performance value ratios is carried out for each problem $p_j \in P$. An advantage in the use of performance profiles lies in the manner this information is visualized in a graph.

In order to understand how a performance profile is drawn, consider the first method, $s_1 \in S$, used to optimize every problem in P . For every one of these problems the ratio of the performance measure value of s_1 in comparison to the minimum value has been calculated. When s_1 has solved the problem best, this ratio is equal to 1. For the remaining problems it is larger than 1. Now, let us consider a certain ratio, indicated by τ_1 . The group of performance measure ratios of method s_1 can be split into two. The first group consists of problems that were solved within a performance value ratio that is less than or equal to this ratio τ_1 . Naturally, the second group is the remaining problems. Every problem in P is contained in one of these two groups. If we now consider another ratio, $\tau_2 > \tau_1$, the number of problems in the first group, thus solved with a ratio no larger than τ_2 , is equal or larger than the number of problems solved within τ_1 . This is due to the tolerance increasing. In a performance profile, the curve of a method indicates the number of problems solved for a range of values of τ . Thus, a performance profile indicates the number of problems a method solved within a certain ratio of the best method among the set. An example of a performance profile can be seen in Figure 5-1. Here the objective function values of three optimizers is compared when optimizing 225 minimum compliance problems using the homogeneous density distribution.

5-2 Performance profiling of initial design influence

In this thesis, the methods being compared are initial design and optimizer combinations. As described in Section 2-1, the problem library used to compare these methods is largely corresponds to the library used by Rojas-Labanda and Stolpe (2015a). The comparison of initial design and optimizer combinations is performed according to the quality and computational cost of the final design. The objective function value of the final design indicates the quality. The cost is proportional to the number of times the system of equations, resulting from the FEM approach, is solved as this is the most expensive part of the TO procedure. It is proportional rather than exactly equal to the number of solves, due to compliant mechanism design

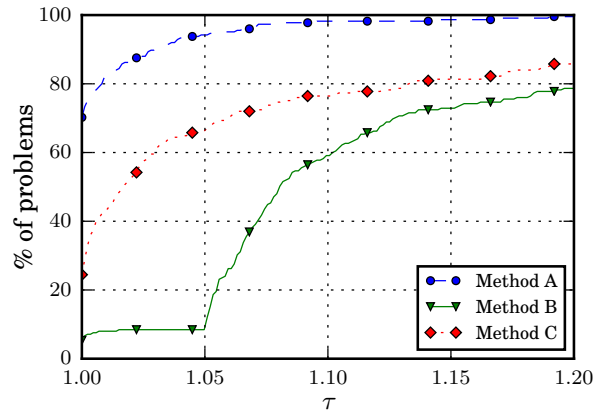


Figure 5-1: Performance profile of three optimizers when tested on 225 minimum compliance problems.

problems requiring the solving of two systems per iteration, but this only being counted as a single solve as these never occur independently.

The cost is the number of times the system of equation is solved as this is the most computationally expensive part of a TO procedure.

In this research, it is desirable of an initial design-optimizer combination to possess three characteristics. Firstly, the solving of the largest amount of problems best. Secondly, the capability to solve the majority of the problems reliably, i.e. consistently good in performance. Finally, the ability to solve any of the problems within a small performance ratio of the best method. Which methods display these characteristics can be observed in a performance profile and are explained using Figure 5-1.

Which method solved the largest number of problems best, is indicated by the percentage of problems a method solves within a factor of $\tau = 1$. Figure 5-1 indicates method *A* solved the largest amount of problems best (approximately 70%). Method *C* follows, solving around 25% of the problems best. According to this first criteria, method *B* performs poorly, solving less than 10% best.

The second desired characteristic, the capability to solve problems reliably, is indicated by a steep increase in the percentage of problems a method solves. This indicates a large number of problems is solved within an approximately equal performance ratio, demonstrating a small spread in the quality. In Figure 5-1 method *B* solves about 50% of problems between $1.05 \leq \tau \leq 1.1$ but only slowly further increases the number of solves problems at larger values of τ .

Finally, the third desired characteristic, the capability to solve any problem well, is indicated by the largest occurring value of τ in the curve of a method.

For all problems, the performance ratio is calculated by dividing the performance of the optimizer considered by the best value among all optimizers, as explained in Section 5-1. The only exception is the compliant mechanism design problems, due to their objective function values being negative. For these problems the performance ratio is calculated by using the inverse of the earlier equation: dividing the best optimizer value by the value of optimizer considered (Rojas-Labanda and Stolpe, 2015a).

5-3 Penalization of inaccurate designs

As described in Section 3-2, an optimizer is stopped when it finds a design that meets the KKT criteria. To prevent optimizers from running indefinitely, a maximum number of solves is also specified. As the required number of solves is one of the two performance measures, the failure to find a KKT-point quickly depreciates the performance of a method. However, it also occurs that optimizers do not meet the problem criteria. The failure of an optimizer to meet these constraints is also reflected in the design its Euclidean norm of the KKT-conditions. If this norm is not below a certain threshold, μ , the optimizer is penalized for that problem (for optimizer specific values of μ the reader is referred to Rojas-Labanda and Stolpe (2015a)). As proposed by (Rojas-Labanda and Stolpe, 2015a), this is performed by assigning it a performance ratio that is slightly larger than the worst occurring value in order to differentiate between optimizers that did not converge and optimizers that converges with the worst performance value. The assigned performance ratio is $1.05f_{\max}$, with f_{\max} being the maximum occurring performance value of all optimizers for that problem. Although this penalization method is subjective, the resulting performance values have a transparent relation with actual values obtained by the optimizers.

5-4 Limitations

Although some comparison difficulties are overcome through the use of performance profiles, there are important limitations. Firstly, optimizers such as MMA are sensitive to the required KKT-norm μ and their curve in performance profiles is heavily influenced by the subjective penalization method. Secondly, the drawn conclusions are only valid for the methods being compared, as the method profiles can drastically change when another method is added to M . That being said, the qualitative behavior among methods does not change. For example, in Figure 5-1 method A will still outperform method C when removing method B , but the differences will be more explicit. Lastly, due to the limited amount of samples, the validity of the conclusions drawn is completely dependent of how the test set represents any problem the methods are expected to solve.

In this research, the question is often: is the difference between two performance profiles significant? The difficulty is that all the previously mentioned limitations influence the answer. As mentioned previously, the difference between two curves can be easily amplified by removing the remaining methods from the profile. Although it is difficult to completely rule out these effects, the investigation of a performance profile is consistently performed using the three desired characteristics as described in Section 5-2 and a detailed description of what is compared is contained in each result section.

5-5 A versatile method to generate performance profiles

For this thesis, a large amount of data is to be analyzed using performance profiles. For that reason a versatile function was written in the high-level, open source, programming language Python. The function, called *gen_perfprof*, is written in such a way that problems,

methods, and performance measure being compared (see Section 5-1) are input variables. In this manner, different perspectives on the data can easily be generated.

The backbone of `gen_perfprof` consists of functions from a package called Pandas. Pandas is an open-source, high-performance, data analysis tool written for Python. Mainly the *groupby* function has come of use. This function enables the splitting of data into groups using which group-specific computation can be performed.

`Gen_perfprof` takes four arguments. The first is the data in the form of a Pandas dataframe, which is a table. The second is the labels which indicate the unique problems in P . The third is the labels which indicate the unique methods, composing S . Lastly, the label which indicates the performance measure, o .

In the `gen_perfprof` the following steps are performed:

1. Find the unique methods.
2. Find the unique problems using the *groupby* function.
3. Apply the normalization by dividing by minimum value or assigning 1.05 times the maximum value (see Section 5-3).
4. Find the unique values of τ .
5. Find the number of solved problems by each unique methods for each occurring value of τ .

This procedure is described using pseudo code in Algorithm 2. During the generation of a performance profile, the data and the resulting profile are checked. These checks consist of the following procedures:

1. Checking if each problem is solved by an equal amount of optimizers. If this is not the case the optimizers solved different problems that cannot be compared (with, for example, differing volume fractions).
2. Inspecting the amount of problems solved at $\tau = 1$. The sum of all optimizer values at $\rho(1)$ is mostly 100%. An exception occurs when there is a problem where optimizers have equal performance values. This occurs, for example, when the maximum allowed number of iterations is violated.
3. Checking the performance measure for negative values. If these are present, unwanted scaling might occur.
4. Inspecting if the number of problems present in the data is equal to the number of (user defined) unique problems multiplied by the optimizers. If this is not the case, possibly unwanted, aggregation of information is taking place.

If a check is not passed, a warning is printed.

5-5-1 Application example

An example follows that demonstrates how `gen_perfprof` allows different perspectives on a single set of data.

Algorithm 2 gen_perfprof

```

1: Input: data, problem definition, performance measure, method characteristic
2:  $S \leftarrow$  unique methods in  $data(method)$ 
3:  $P \leftarrow$  unique problems in  $data(problemdefinition)$ 
4: for  $p$  in  $P$  do
5:   if  $feasibility$  is TRUE then
6:      $o_{p,s} \leftarrow \frac{o_{p,s}}{\min(o_{p,s} \forall s \in S)}$ 
7:   else
8:      $o_{p,s} \leftarrow 1.05 * \max(o_{p,s} \forall s \in S)$ 
9:  $\tau_{\text{uniq}} \leftarrow$  unique  $o_{p,s} \forall p \in P, \forall s \in S$ 
10: for  $\tau$  in  $\tau_{\text{uniq}}$  do
11:   for  $s$  in  $S$  do
12:      $\rho_{s,\tau} \leftarrow \frac{\text{size}(o_{P,s} \geq \tau)}{\text{size}(P)}$ 
13: Return:  $\tau_{\text{uniq}}, \rho_{s,\tau}$ 

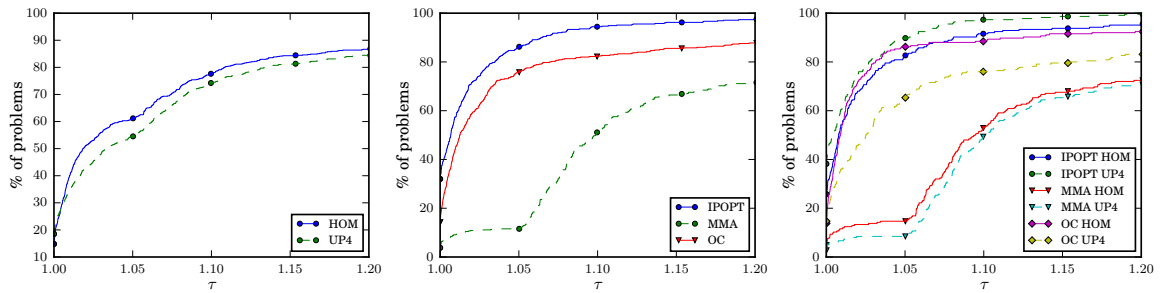
```

Table 5-1: Final objective function value, number of iterations, solves, and feasibility fo three optimizers and two IDs for one of the minimum compliance problems.

nelx	nely	vol.	prob. type	optimizer	ID	obj.	iter.	solves	feas.
120	60	0.1	Cantilever	IPOPT	HOM	494	1000	1140	True
120	60	0.1	Cantilever	IPOPT	UP4	484	340	362	True
120	60	0.1	Cantilever	MMA	HOM	712	1000	1000	False
120	60	0.1	Cantilever	MMA	UP4	497	1005	1005	False
120	60	0.1	Cantilever	OC	HOM	501	1000	1000	True
120	60	0.1	Cantilever	OC	UP4	483	1005	1005	True

Consider the 225 minimum mechanical compliance problems described in Section 2-1-1. The performance of the three optimizers using HOM and UP4 as initial designs is indicated for a single problem in Table 5-1.

Figure 5-2 contains three performance profiles, generated using the minimum compliance problems. For every profile the problem definition is the same, set by the labels [nelx, nely, volfrac, problem type], but the definition of a unique optimizer varies. In Figure 5-2a, the methods, M , are defined by the unique initial designs, see Table 5-1. Each curve contains the information of all three unique optimizer (thus OC, MMA, and IPOPT), and contains 675 data points. This figure indicates that, when aggregating the performance of all optimizers, HOM outperforms UP4. Now, in Figure 5-2b, the methods are defined by the unique optimizers, each curve representing 450 data points. This figure indicates IPOPT is the best optimizer. Finally, Figure 5-2c contains the profiles of each unique initial design and optimizer combination. As each unique combination has optimized 225 problems, the curves represent 225 data points. This profile indicates that IPOPT performs better when initialized with UP4 than with HOM, and OC and MMA do not.



(a) Sorting by the unique initial designs. (b) Sorting by the unique optimizer. (c) Sorting by the unique initial design optimizer combinations.

Figure 5-2: Performance profiles of the objective function value for the 225 minimum compliance problems with different definitions of a unique method.

Numerical experiments results for initial designs

In the first numerical experiments a test set of three problem classes containing a total of nine problem types are used to assess the value of the different initial design and optimizer combinations. In order to be able to elaborate more extensively on the important results, this section only contains a subset of all performance profiles. Appendix E contains all profiles of all problem classes.

The performance measures are the final objective function value and total amount of stiffness matrix assemblies, as described in Section 5-2. Only the profiles of the minimum compliance and compliant mechanism design problems are contained and explained in this chapter. The results of the minimum volume problems are similar to the results of the remaining experiments while the differences between the performance of initial designs is smaller. The profiles can be seen in Appendices E and E. Lastly, the performance profiles do not contain all combinations of methods in order to maintain readability of the profiles. An explanation of the selection procedure follows.

The choice has been made to mostly compare the homogeneous density distribution (HOM) with one other initial design using all optimizers. The other initial design is often chosen to be the one that has the best performance for the best optimizer. Problem specific details are contained in the appropriate sections.

When qualitatively comparing the performance of the optimizers using the HOM with the results of Rojas-Labanda and Stolpe (2015a), similar trends are observed. A quantitative comparison cannot be performed due to the different sizes of the problem sets and the performance profiles containing different methods.

6-1 Minimum compliance problems

For the mechanical compliance problems the tested initial designs include HOM and the optimized unpenalized problem (UP) using three different mesh sizes. The results indicate

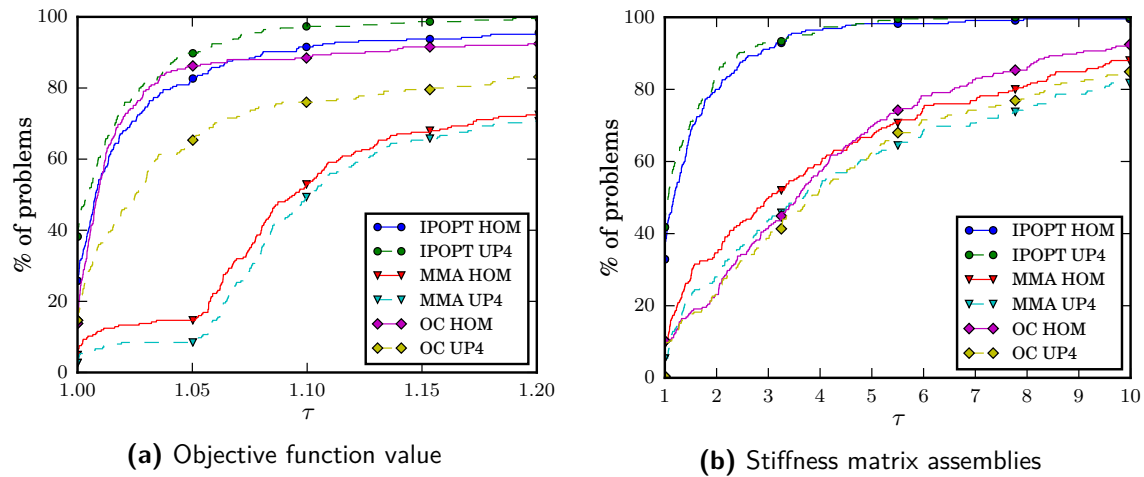


Figure 6-1: Performance profiles for the 225 minimum compliance problems.

that the performance of both OC and MMA deteriorates using the unpenalized initial designs. The performance of IPOPT is either similar or better when using UP. Amongst these, a course mesh, combining sixteen finite elements of the original mesh to one element for the unpenalized problem, performs best. Thus UP4 is compared to HOM for all three optimizers in Figure 6-1. A quantitative analysis follows.

IPOPT using UP4 is the best overall method. Regarding the objective value, it solves 38% of all problems best (at $\tau = 1$), 12% more than the next best (IPOPT using HOM). IPOPT using UP4 solves the most problems across the whole spectrum of τ , solving 100% of problems within $\tau = 1.27$ in comparison to $\tau = 16.9$ for IPOPT HOM. Regarding OC the number of problems solved best using UP4 in comparison to HOM lies 1% higher the remaining spectrum of τ indicate a large decrease in performance. The performance of MMA is generally poor due to it being penalized for not properly converging to a KKT point. When using HOM this only occurs in 15% of the problems and further deteriorates to 8% using UP4.

Figure 6-1b shows that IPOPT also outperform OC and MMA regarding the number of stiffness matrix assemblies. IPOPT UP4 solves 42% of problems best, 9% more than IPOPT HOM. Furthermore, a slightly lower amount of stiffness matrix assemblies is required when using UP4 than when using HOM for all but a small part of the τ spectrum. However, the difference is not very significant. IPOPT UP4 solves all problems within $\tau = 6.55$ in comparison to $\tau = 11.24$ for IPOPT HOM. OC and MMA their convergence performance is worse when using UP4.

6-2 Minimum thermodynamic compliance problems

For the minimization of thermodynamic compliance, Constructal Theory (CT), an approximate solution to the unpenalized problem, and HOM are used as initial designs. Four variations of the CTID are tested. Each one with a larger density difference between the CT shape and the remainder of the design domain, dictating how explicitly the CT shape is present in the initial design (for details see Section 4-2). How this explicitness affects the final design can be seen in Table 6-1. The images indicate that, when using OC and MMA, the final

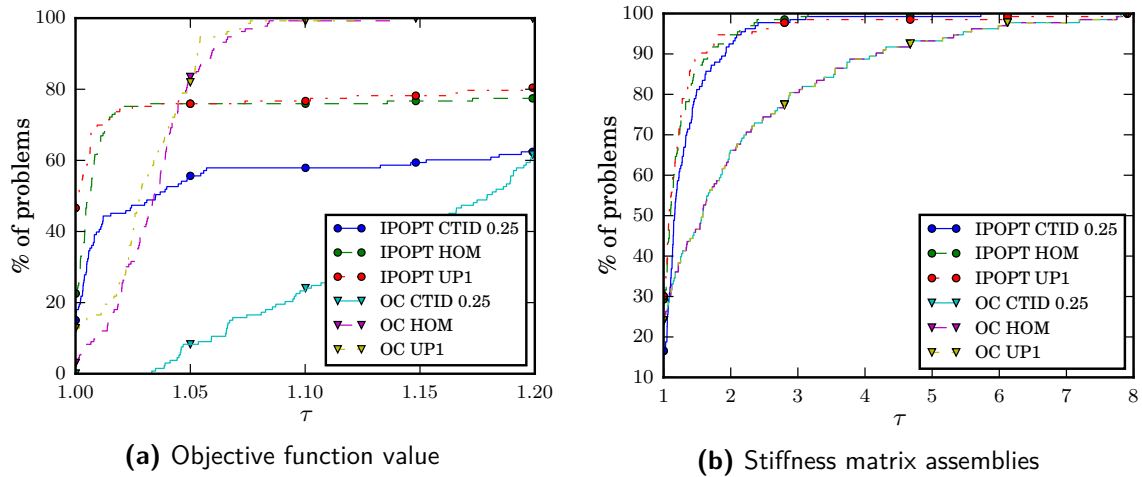


Figure 6-2: Performance profiles for the 133 minimum thermodynamic compliance problems.

result resemble the CTID more as it is more explicitly present. The IPOPT results do not display this tendency. Of all designs no two are equal, indicating that each design represents another minima.

Figure 6-2 displays the performance profiles for the minimum thermodynamic compliance problems. These contain the curves of three initial designs types combined with two optimizers. Regarding CT, the initial design with a density difference of 0.25 is chosen due to this being the best performing of the CTIDs (for all CTIDs see Appendix E). Regarding the optimizers, MMA is not plotted due to poor performance. This is due to the poor convergence to KKT points, which occurs independently of the used initial design.

Regarding the objective function value, CT performs worse than the HOM for both OC and IPOPT. Comparing UP1 to HOM, the number of problems solved best increases from 23% to 47% for IPOPT and from 3% to 13% for OC. Figure 6-2a indicates IPOPT either performs a competitive design or a poor design, as also observed in (Rojas-Labanda and Stolpe, 2015a). For $\tau > 1.05$ OC outperforms IPOPT, solving 100% of problems at $\tau = 1.12$ for UP1 and $\tau = 1.14$ using HOM.

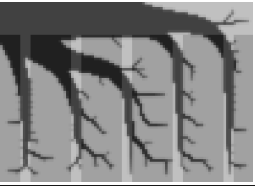
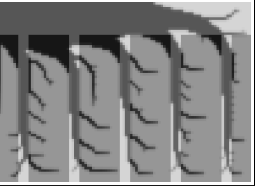
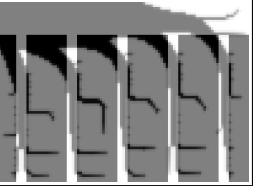
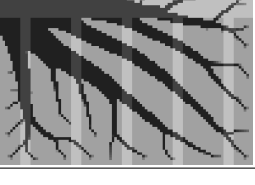
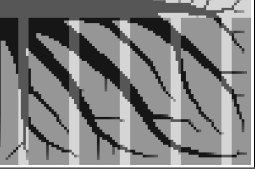
When inspecting the number of solves, Figure 6-2b indicates that the initial design has no influence on the number of solves required by OC. IPOPT solves 80% of problems within $\tau = 1.31$ using UP1 in comparison to $\tau = 1.39$ for HOM and 1.49 for CT 0.25. However, 100% of problems are only solved within $\tau = 7.91$ using UP1 in comparison to $\tau = 3.15$ for HOM and 5.75 for CT 0.25.

6-3 Compliant mechanism design

Figure 6-3 contains the performance profiles for the compliant mechanism design problems. It was chosen to compare UP4 with the HOM due to its high performance and low computational cost.

In general, the performance using UP4 is comparable or better than the performance using HOM. The number of problems solved best is equal in both cases when using IPOPT, while

Table 6-1: Density difference between the initial design and the final solution to the minimum thermodynamic compliance problem with volume fraction of 0.35. White areas indicate where the initial design contains more material than the final design, gray areas indicate where the two have an equal density while black areas indicate where the final solution has a higher density than the initial design. The CT initial design shape is always equal. The columns indicate the density difference present in the CTID.

Optimizer	Initial design			
	HOM	CTID 0.25	CTID 0.5	CTID 1
OC				
MMA				
IPOPT				

for OC the percentage increases from 12% to 21%. OC using UP4 is generally the best method, solving 80% of problems within $\tau = 1.06$, followed by OC HOM which does this in $\tau = 1.08$. Furthermore, all problems are solved by OC UP4 within $\tau = 1.46$ compared to $\tau = 2.03$ for HOM. IPOPT produces either a well performing design, or a very poor design. This is visible when comparing the τ values when solving 80% and 100% of problems. Using UP4 and HOM, 80% of problems are solved within $\tau = 1.09$ and $\tau = 1.17$ while the maximum occurring τ values are 1585 and 646.

Regarding the number of stiffness matrix assemblies, IPOPT is the best general optimizer. The percentage of problems solved best by IPOPT increases from 28% to 31% for IPOPT when using UP4 instead of HOM while for OC it decreases from 30% to 1%. IPOPT UP4 solves 80% of problems in $\tau = 1.55$ instead of $\tau = 1.86$ when using UP4 while the largest occurring ratio amongst all problems is reduced from 20.1 to 14.5.

6-4 Initial design performance discussion and conclusion

Comparing all initial design and optimizer combinations, one can conclude that there is not a single initial design that outperforms all others for all problems. Moreover, when considering a specif problem class, the performance of an initial design is optimizer dependent. That being said, the unpenalized initial design generally performs well when compared to the homogeneous density distribution regarding the final objective function value. Regarding the

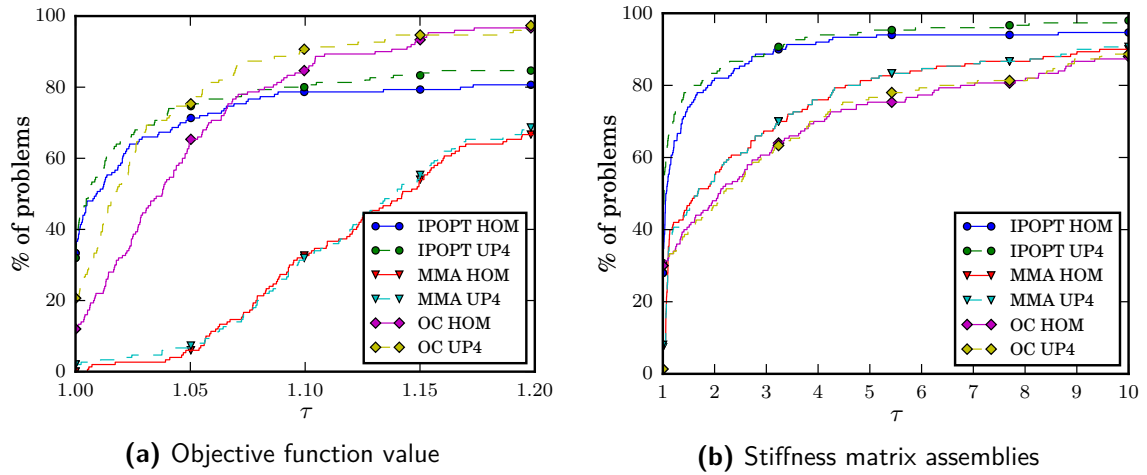


Figure 6-3: Performance profiles for the 150 compliant mechanism design problems.

number of solves, the performance of UP is comparable to HOM. The designs obtained using Constructal Theory perform poorly, independent of how explicit this initial design is present, and independent of the optimizer used.

As observed by Rojas-Labanda and Stolpe (2015a) IPOPT generally performs very well. A clear difference in results is that IPOPT is also competitive with MMA and OC when inspecting the number of solves. This might be an attribute of the used test set of each problem class being larger. OC is generally competitive, although sensitive to the initial design used. On the other hand MMA performs poorly due to it being penalized in a large number of problems due to insufficient convergence to a KKT point. The KKT error mostly consists of the stationary conditions being unsatisfied, which is a result of MMA being a first order method. When not applying this penalization, MMA UP generally outperforms MMA HOM, as visible in the profiles in Appendix E.

As UP can be considered a continuation method with a single steep step in the penalization parameter, the observed increase in performance is in agreement with the generally observed increase in performance when using continuation methods.

Table 6-2 contains problem specific recommendations regarding the use of initial design optimizer combinations. An important reminder is that not all optimizer initial design combinations are investigated for all problems, for an overview see Table 2-1.

Table 6-2: Recommended initial design optimizer combinations regarding the objective function value and number of solves.

Problem class	Objective	Iterations
Minimum mechanical compliance	IPOPT UP4	IPOPT UP4
Minimum thermodynamic compliance	OC UP1	IPOPT HOM
Mechanical minimum volume	IPOPT UP1	IPOPT HOM
Thermodynamic minimum volume	IPOPT UP1	IPOPT HOM
Compliant mechanism	OC UP4	IPOPT UP4

Numerical experiments results for optimizer robustness

In the second set of numerical experiments the robustness of the three optimizer is investigated. This is done by generating a poorly performing initial design and comparing the final result with the result when using HOM as an initial design. For brevity, only the profiles with respect to minimum mechanical compliance and compliant mechanism design problems are shown. The conclusions drawn from the minimum volume problems do not differ from the conclusions drawn below.

The robustness of optimizers is analyzed using the most significant of four measures. Firstly, the change in percentage of problems solved best. Secondly, the value of τ when solving 80% of the problems, thirdly the maximum occurring value of τ , and finally the change in percentage of feasible solutions.

7-1 Minimum compliance problems

Figure 7-2 contains the profiles for the minimum mechanical compliance problems. An example of a BAD initial design can be seen in Figure 7-1a. It contains the BAD initial design as generated for the two by one Cantilever with 10% volume fraction. Figures 7-1b-7-1d display the differences in the final design obtained by the BAD initial design compare to HOM.

Figure 7-2a indicates that the varying amount the BAD initial designs affect the final objective function value. The performance of the OC optimizer is severely affected, with the 80% of the problems being solved within $\tau = 1.11$ instead of $\tau = 1.02$. Furthermore, the percentage of feasible designs drops from 100% to 60%. Interestingly, the largest occurring value of τ is reduced slightly when using the BAD initial design, although not by a significant amount. Even though the profiles of IPOPT are visually similar, the percentage of problems solved best is reduced from 31% to 24% when using the BAD initial design. Somewhat surprising in the large reduction in the value of τ required to solve all problems, being reduced from

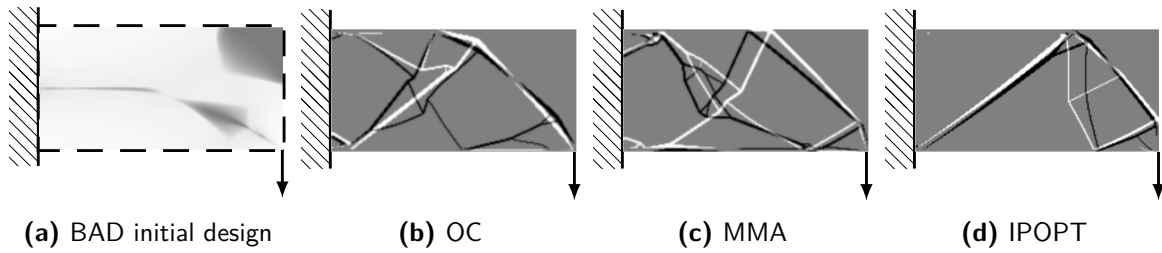


Figure 7-1: Example of a BAD initial design and optimizer specific results. Black elements indicate the presence of material in the final design when using HOM that is not present in the final result when using the BAD initial design. White elements indicate the opposite. Grey areas indicate where the designs do not differ.

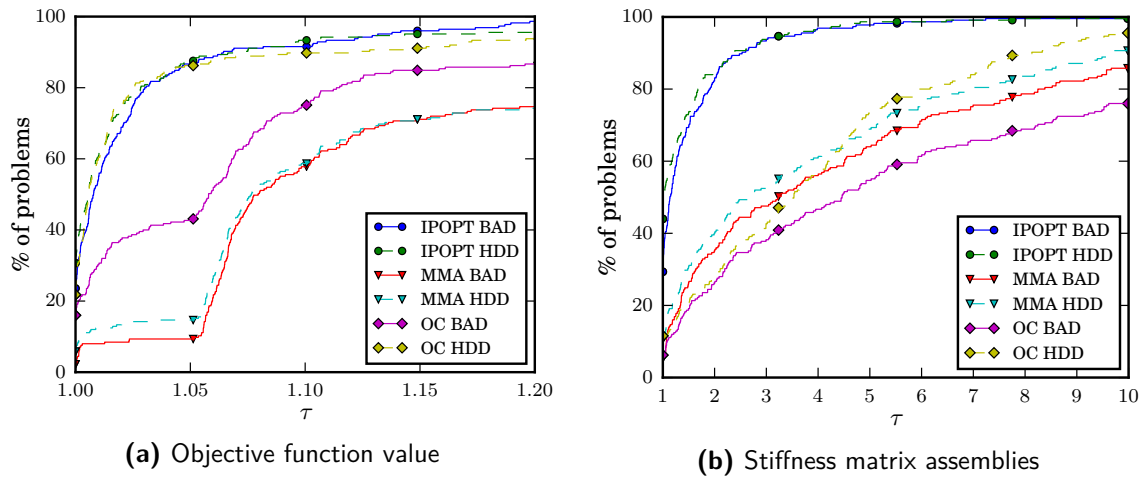


Figure 7-2: Performance profiles for the 225 minimum compliance problems when using HOM and BAD initial design.

$\tau = 16.78$ for HOM to $\tau = 1.25$ using BAD, even though all final results are feasible in both cases. MMA its number of feasible solutions is reduced by 4% to 2%. For larger values of τ the curves do not differ much from each other due to the heavy penalization.

Regarding the number of solves, again the performance of OC is severely affected. The performance ratio when solving 80% of the problems increases from $\tau = 5.96$ to $\tau = 13.51$ while the last problem is solved at $\tau = 35.71$ instead of $\tau = 14.93$ for HOM. As in the objective function value, IPOPT is hardly affected. The percentage of problems solved for the range of τ values lies a steady 5% lower when using BAD in compared to HOM.

7-2 Compliant mechanism design

Figure 7-3 contains the profiles of the optimizers using the HOM and BAD initial designs for compliant mechanisms. The BAD initial design is generated using the IPOPT optimizer with a maximum number of 90 iterations. A visual inspection of these initial designs indicate the consequences of this choice. Especially the designs with a large amount of elements contain many gray elements. When observing the iteration history of IPOPT, it is clear that a binary

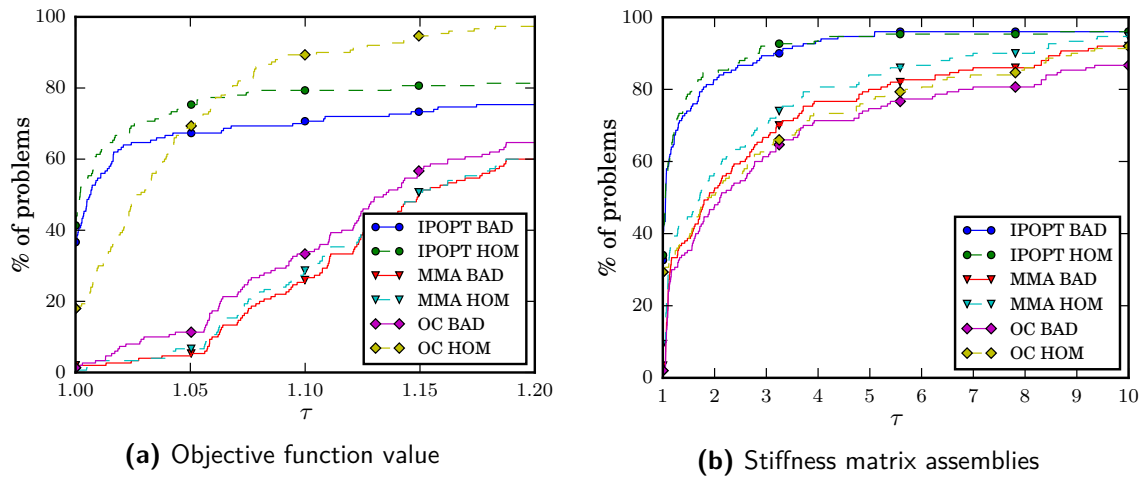


Figure 7-3: Performance profiles for the 150 compliant mechanism when using the homogeneous density distribution (HOM) and BAD initial design.

design is achieved relatively late in the design process. This is in contrast to, for example, OC, that emerges with a binary designs within 100 solves. Even though the BAD initial designs do not explicitly contain a mechanism, large differences in performance between the HOM and BAD initial designs can be observed.

Regarding the objective function value, the performance of each optimizer is reduced when using the BAD initial design in comparison to the HOM. The performance of OC is most heavily affected, with the percentage of feasible designs dropping from 100% to 13%. After solving 80% of problems within a factor $\tau = 2.78$ for the BAD initial design instead of $\tau = 1.07$ for the HOM, the increase of solved problems occurs very slowly for the BAD initial design. This indicates a large spread in the remaining problems their performance ratio. The largest performance ratio, $r_{p,OC}$, increases from 1.7 to 3567. The convergence of IPOPT is reduced from 95% to 89% while it solves 80% of problems at $\tau = 1.34$ instead of $\tau = 1.14$. The number of problems solved also increase very slowly and it solves its last problem at a performance ratio of 3567 in compared to 588 for the HOM. The percentage of feasible designs generated by MMA is reduced from 9% to 5% and the performance curves are similar.

Regarding the number of solves, the earliest mentioned percentages of feasible designs also indicate the decrease in number of problems where the optimizer terminated before reaching the maximum number of solves when using the BAD initial design. Figure 7-3b indicates that all optimizers their required number of solves increases when using the BAD initial design in comparison to the HOM.

7-3 Optimizer performance discussion and conclusion

The numerical experiments indicate large differences in the capabilities of optimizers to handle poorly performing initial designs. IPOPT is generally capable of generating a final design that performs well when compared to IPOPT HOM. An explanation can be found in the knowledge that interior point methods are generally insensitive to ‘warm starts’ (Forsgren, 2006). These are used when the optimal solution to a particular problem is known, and another problem,

resembling the first one, is to be optimized. In the experiments the performance of OC is severely affected by the BAD initial design. Lastly, the impact of the performance on MMA is hardly visible, although the percentage of feasible results is further reduced.

Chapter 8

Discussion

Although the problems, initial designs and optimizers were chosen with the aim of forming a representative investigations there are many limitations. Firstly, only the SIMP formulation using a single filter type is applied. Secondly, the optimizer settings are chosen to equal the ones used by Rojas-Labanda and Stolpe (2015a). This was done due to optimizers being generally sensitive to these settings, and an investigation of the optimal setting requiring a lot of time. Finally, the test set contains only 2D examples.

The remaining part of this chapter investigates when a difference between two performance profiles is significant and for which mechanical compliance problems the IDs performed the poorest.

8-1 On when performance curves differ significantly

When comparing two curves in a performance profile, a large distance between the curve naturally indicates large differences in performance. Even though the profiles presented in Chapter 6 and 7 are systematically analyzed, the question that remains is: when are two profiles significantly different? Or: in what sense is some method *A* slightly outperforming method *B* a matter of chance? As discussed in Section 5-4, this depends on multiple factors. One of the factors is the chosen test set, and a single experiment is performed in order to investigate the effect of this factor.

The validity of a the conclusion resulting from the analysis of a performance profile is wholly dependent on how the test set represent the problems a method is expected to solve. One approach to investigate the consistency of a method is by comparing the performance profiles when optimizing random subsets of problems. This has been performed for the 225 mechanical compliance problems, with the subsets consisting of the 95% of problems with worst and best performance ratio. Figure 8-1 contains the resulting performance profiles. The subsets naturally form an upper and lower bound around the curve.

Any random subset containing 95% of the problems must lie in between the indicated bounds. Naturally, the width of the band is a function of the gradient. Consider the profile indicating

the objective function value in Figure 8-1a. The lower bound of the IPOPT UP4 profile lies above the upper bound of the IPOPT HOM profile for $\tau < 1.1$, which is an indication of the optimizer robustness. A clearer, quantitative definition of the significance in the difference in such curves has not been found and further investigations is recommended.

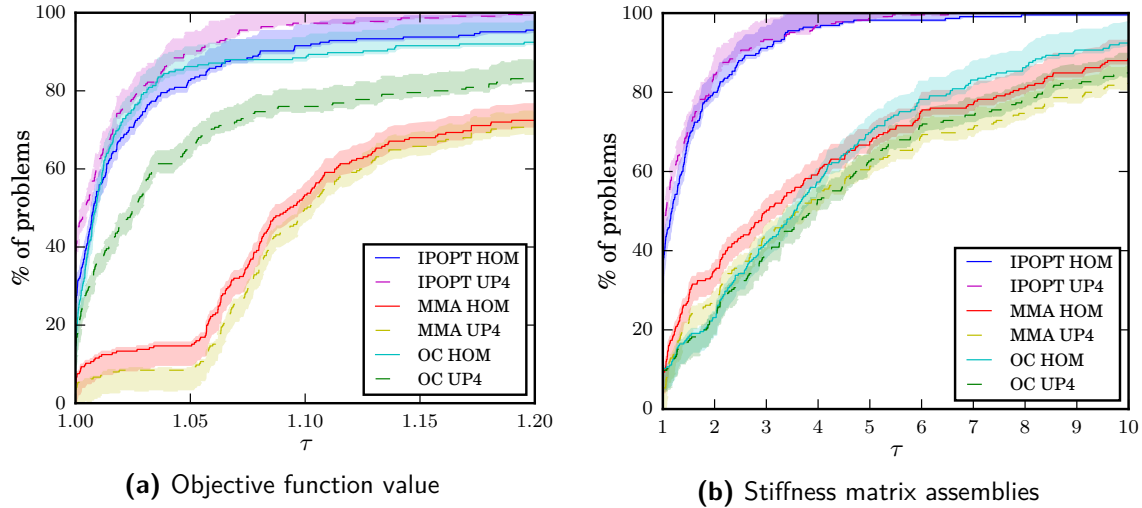


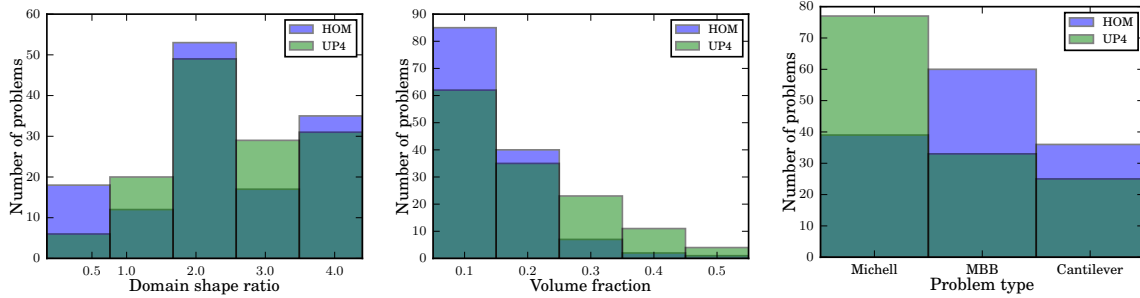
Figure 8-1: Performance profile for the 225 minimum compliance problems including bounds indicating the curves of the 95% worst and 95% best problems.

8-2 Learning from the data

The numerical experiments required the optimizing of a large number of problems. In addition to the performance comparison performed in the previous chapters, the resulting data contains valuable information. Examples of questions that arose during the analysis are:

1. Can the solution to the unpenalized problem be used to indicate how close the results are to the global optimum?
2. Why does the OC optimizer not benefit from UP for only mechanical compliance problems?
3. Compliant mechanism design problems are generally more difficult than minimum compliance problems. Is the difference obtained by using UP as an initial design also larger?
4. For which problems do the optimizers obtain the largest performance ratios?
5. For which problems do the initial designs obtain the largest performance ratios?
6. Do the difficult problem types differ for the initial designs?

In this section the last two questions are addressed. This is done by analyzing the results obtained for the mechanical compliance problems. The first step is the calculating of the performance ratios according to the objective function value or number of solves, as done when drawing a performance profile. The difference is now that a penalization of infeasible results is not applied. In this case, the methods distinguish themselves according to the ID used (for details see Section 5-5-1), thus all optimizer information is aggregated into one



(a) Considering the domain shape/aspect ratio. (b) Considering the volume fraction. (c) Considering the problem type.

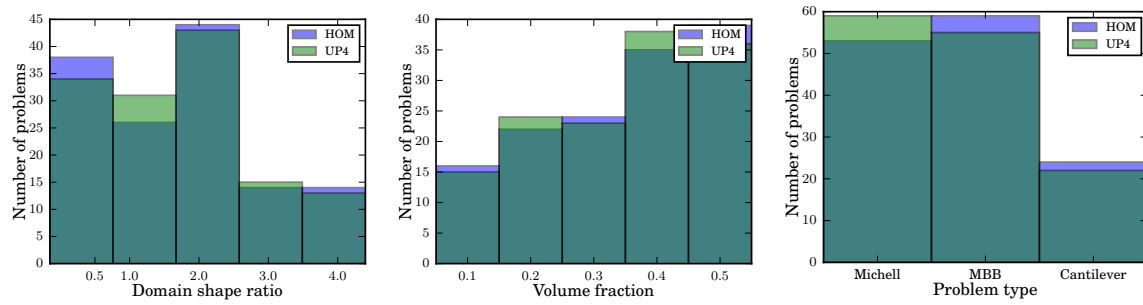
Figure 8-2: Distribution of the 20% of problems with the largest objective function value ratios for different parameters. The performance of the different IDs is compared, aggregating the solvers.

curve. Then the 20% of problems with highest τ values are selected. Lastly, these problems are plotted in histograms.

An important note is to be added regarding the aggregation of information. Through this definition the best optimizer ID combination performance value is selected and the remainder of combination ratios is calculated. This is the same as when distinguishing between unique optimizer and ID pairs. The difference now is that all optimizers are aggregated. The plots thus also reflect the performance of the optimizers, but with respect to the influence of the IDs. Considering the 20% of most difficult problems when optimizing using UP4, it is possible that OC and MMA are be part of this curve for a single problem, while IPOPT solved the problem best, even in comparison to the results obtained using HOM. In this manner, the capability of an ID to improve the performance of all optimizers is analyzed.

Figure 8-2 contains histograms of the difficult problems when considering the objective function value. Figure 8-2a indicates problems with a larger aspect ratio (being long and slender) are generally more difficult to solve, although the trend is not definite. The trend is more explicitly present for UP4 than for HOM. On the other hand, Figure 8-2b clearly indicates that problems with a smaller volume fraction are more difficult. The figure indicates that when using UP4 the problems are slightly more uniformly distributed. Interestingly, Figure 8-2c indicates the Michell truss problems being particularly difficult when using UP4, the 20% of problems containing almost twice as many Michell truss problems as any other.

Figure 8-3 contains histograms of the difficult problems when considering the number of solves. The differences between the initial designs is less explicit than when considering the final objective function value. Interestingly, large volume fractions required a larger number of solves.



(a) Considering the domain shape/aspect ratio. (b) Considering the volume fraction. (c) Considering the problem type.

Figure 8-3: Distribution of the 20% of problems with the largest number of solves ratios for different parameters. The performance of the different IDs is compared, aggregating the solvers.

Conclusion and future work

In density based TO, the choice of the initial design is a key parameter, affecting both the quality of the final result and computation required to reach convergence. In this thesis, a method to systematically investigate these effects has been applied to four initial design generation methods for the first time in the TO community. The analysis method consists of optimizing a large, diverse set of benchmark problems among three problem classes and analyzing the results using performance profiles.

The main objective of this research is the performance comparison of two ID generation methods with HOM, which is now commonly used. The results indicate that no ID outperforms all others for all problems. Furthermore, the performance of an ID is optimizer dependent. The Constructal Theory inspired initial design performs poorly. The approximate solution to the unpenalized problem generally outperforms HOM. The generally best performing optimizer, IPOPT, benefits from UP when optimizing for minimum compliance, minimum volume, and compliant mechanism design. This is mostly independent of the mesh coarseness the ID is generated on, while the largest performance increase is often observed using a coarse mesh. OC and MMA also perform better when using UP than HOM, although they require the mesh to be as fine as the original problem, resulting in a higher computational cost than HOM. Considering UP as a continuation method with a single, steep step in the penalization parameter value, the decrease in objective function value agrees with the results obtained when using continuation methods.

The secondary research objective consists of investigating the robustness of optimizers to poorly performing IDs. The results indicate IPOPT is generally very robust, generating designs comparable to ones obtained when initiated with HOM, at similar computation costs. This is an attribute to interior point methods being insensitive to warm starts. The performance of OC is severely affected regarding both the quality and required computation. As in the investigation of different IDs, the performance of MMA is generally poor due to the inability to converge to a KKT-point. This is an attribute of it being a first order method.

Future work

The validity of the numerical experiment conclusions can be investigated further. The generation of performance profiles including a certain percentage of worst and best solved problems might be an approach. Furthermore, the significance of results is a subject profoundly studied within the area of mathematical statistics. A study of these methods can be of use in order to quantify the difference between similar performance curves.

Through the optimization of the large and diverse set of problems, a huge amount of data was generated. For example, the iteration history contains the objective function value, change in design between iterations and value of the KKT conditions. A detailed data analysis of these results is recommended as this undoubtedly results in knowledge about the optimizers and problems.

One would expect the performance of IDs to differ more when the tested problems become more difficult. The application of UP to, for example, large 3 dimensional problems with multiple loads might further confirm it being a well performing ID.

Finally, it would be interesting to compare the performance of problems initiated with the UP ID to the use of continuation methods. The latter methods generally require a large number of iterations and UP might be an interesting alternative, improving the objective function value at limited computational cost.

Difficulties in Topology Optimization: mathematical background

This appendix contains a sketch of why TO problems are difficult from the perspective of complexity theory followed by the definition of convexity.

A-1 Computational complexity theory

TO problems are known to be difficult problems in general Bensøe and Sigmund (2003). In this section, the level of this difficulty is described more precisely using computational complexity theory.

In the field of computational complexity theory, mathematicians and computer scientists aim to classify computational problems according to their inherent difficulty, and relate these classes to one another. Many different types of complexity classes have been identified, and a simple type of TO problem, namely a truss-sizing problem, has been proven to lie in one of these classes Yates et al. (1982).

Both the computational complexity of the problem classes and the presence of TO there are mathematically precisely defined but lie outside the scope of this text (the interested reader is referred to Garey and Johnson (1990)). Simply speaking, the truss-sizing problem is proven to lie in a particular complexity class by proving that a problem that lies in this class can be formulated as a truss-sizing problem. The solution to this newly formulated truss-sizing problem can be mapped back to a solution of the original problem. Finding the solution to the truss-sizing problem can thus only be at least as difficult as solving the original problem, indicating the difficulty of solving truss-sizing problems. With regards to the complexity of the problem class, TO problems are very difficult optimization problems indeed. This is due to the number of possible solutions that need to be evaluated to find the global minimum being proportional to the size of the solution set.

Even without a precise understanding of the mathematical complexity of TO problems there is a clear message: finding the global minimum is not possible in a practical amount of time.

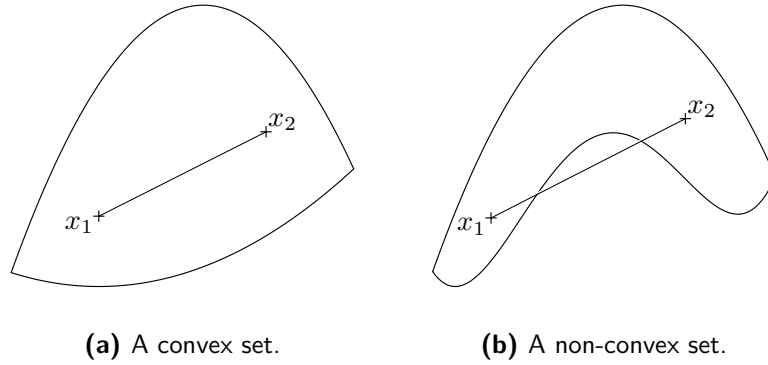


Figure A-1: Two sets in \mathbb{R}^2 .

This is due to TO problems naturally containing a large amount of variables. Evaluating even a fraction of the possible solutions is impossible for anything but the smallest problem sizes (e.g. Rasmussen and Stolpe (2008)).

A-2 Convexity: to be or not to be

The presence of local minima in the domain of a function is described by a general mathematical property, namely *convexity*. This section contains the definition of convexity and some associated properties. Before defining a convex function, let us investigate the definition of a convex set.

Definition A.1. Consider a set \mathcal{C} of points x_i with $x_i \in \mathbb{R}^n \forall x_i \in \mathcal{C}$. Let $0 \leq \lambda \leq 1$ be given. A convex combination of two points, $\{x_i, x_j\}$, is defined as $x^* = \lambda x_i + (1 - \lambda)x_j$. Finally, the set \mathcal{C} is convex if all convex combinations of the points $\{x_i, x_j\}$ again lies in \mathcal{C} : $\{x^*(x_i, x_j) \in \mathcal{C} | \forall \{x_i, x_j\} \in \mathcal{C}\}$.

A geometric interpretation follows. Consider the convex set of points $\{x_i\} \in \mathbb{R}^2$ defining the polygon in Figure A-1a. The set is convex by definition A.1 due to any point lying on the line between two points, x_1 and x_2 , also lying in the set. Thus, when moving from one to another point in the set, only points inside the set are encountered. This is not the case for the non-convex set visible in Figure A-1b. Pairs of points exist where the line between the two points does not fully lie inside the set.

The definition of a convex function follows.

Definition A.2. A function $f : \mathcal{C} \rightarrow \mathbb{R}$ defined on a convex set \mathcal{C} is convex if for all $\{x_i, x_j\} \in \mathcal{C}$ and $0 \leq \lambda \leq 1$: $f(\lambda x_i + (1 - \lambda)x_j) \leq \lambda f(x_i) + (1 - \lambda)f(x_j)$.

A geometric interpretation using Figure A-2 follows. The solid line indicates the value of f for $f(\lambda x_1 + (1 - \lambda)x_2)$. The dotted line indicates the value of the function $\lambda f(x_1) + (1 - \lambda)f(x_2)$. As the solid line is less than or equal to the dotted line for $0 \leq \lambda \leq 1$, the function is convex. Let us inspect the solution topography of f with regard to local minima. As visible in Figure A.2, the function f contains only one minimum, it naturally being the global minimum. Now

consider the non-convex function visible in Figure A-2b. By definition A.2 it is clearly not convex. Furthermore, there are two minima present. The right minimum with $\lambda \approx 0.9$ is a local minimum while the minimum at $\lambda \approx 0.1$ is the global minimum due to there not being any other value of f that lies below this value. Thus, convex function contain only one, global, minimum while non-convex function contain multiple minima.

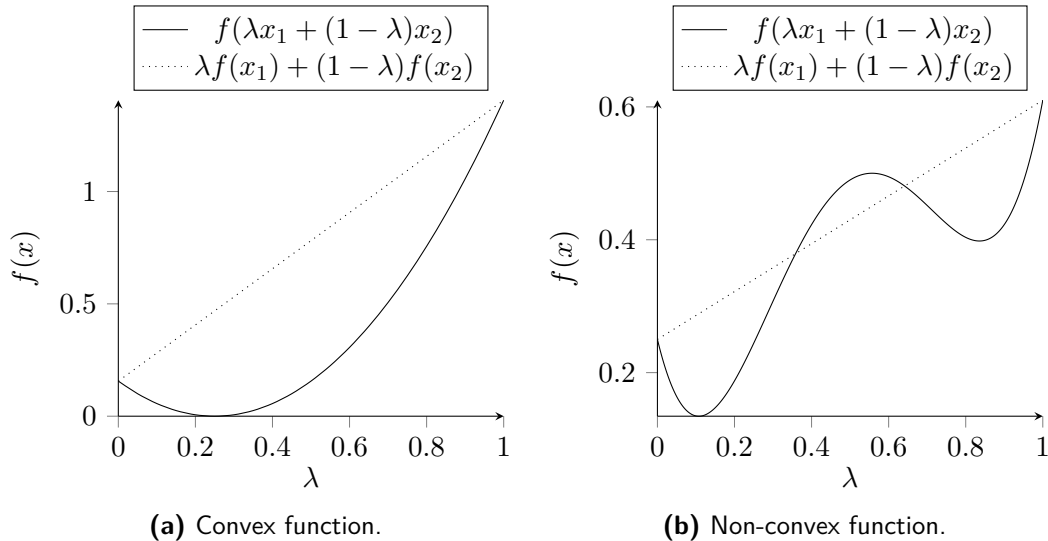


Figure A-2: Functions

The question arises of how to discover if a function is convex or not. One could map different points on the solution topography and test for convexity using definition A.2 but this is tedious and possible endless. Other definitions of convexity make this unnecessary. Consider again figures A-2. The derivatives of the functions $f_{\text{conv.}}$ and $f_{\text{nonconv.}}$ are clearly different. The values of $\frac{\partial f_{\text{conv.}}}{\partial \lambda}$ are all positive while the sign of the values of $\frac{\partial f_{\text{nonconv.}}}{\partial \lambda}$ differs on different part of the function domain. This is generalized in the following, alternative, definition of a convex function.

Definition A.3. A function $f : \mathcal{C} \rightarrow \mathbb{R}$ defined on a convex set \mathcal{C} is convex if the gradient ∇f is monotonically increasing.

A function g is monotonically increasing if for two points, where $x_1 < x_2$, it hold that $g(x_1) < g(x_2)$.

Appendix B

Constructal Theory details

The aim of this appendix is to explain Constructal Theory (CT) in detail. Although considerable time and effort has been spent to explain CT clearly and concisely, this appendix might not change the perception of the reader that CT is a messy and vague theory. The author can only remark that, even after extensively studying CT, he has the same feeling. In the first section the original CT is described. The results of this theory have been calculated in more precisely and the second section highlights these modifications. The CTID, as explained in Section 4-2, is generated using these modified equations. The section ends with general remarks.

The derivation of many of the equations in this appendix can be found in appendix C. These have been separated from this text with the aim of improving readability. When a derivation has been performed, a reference is placed in the text.

B-1 The original CT

CT generates a solution to the volume to point flow problem by assembling an elementary, also called the zeroth order, element into higher order designs. This process is dictated by the value of the two input variables, the ratio of conductivity \tilde{k} and the volume fraction of high-conductivity material ϕ . The resulting CT design defines the ratio between the height, H , and length, L , of the design domain, and the placement of the high conductivity material. In this section the equations defining the critical shapes of the zeroth, first, and second order elements are explained. For details on the volume-to-point flow problem the reader is referred to Section 4-2.

B-1-1 Zeroth order element

In CT, the zeroth order element is the smallest building block where the feature size is dictated by manufacturing constraints. In this element, the high conductivity material is

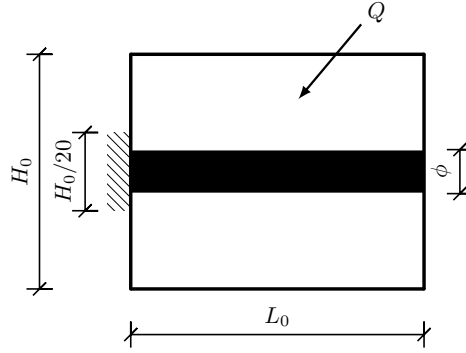


Figure B-1: Elementary construct.

always present as a rectangular shape, running from the heat sink to the other end of the domain. An example of an elementary construct is visible in figure B-1.

The thickness of the blade, D_0 , is naturally proportional to the volume fraction of material allocated to this element: $D_0 = \phi_0 H_0$. The value of the ratio $\frac{H_0}{L_0}$ is chosen in order to minimize the maximum temperature difference ΔT_0 between the heat sink and the upper and lower right corners. This temperature difference is approximated in dimensionless form using

$$\frac{\Delta T_0 k_0}{q''' A_0} = \frac{H_0}{8L_0} + \frac{1}{2\tilde{k}\phi_0} \frac{L_0}{H_0}. \quad (\text{B-1})$$

The right hand side consists of two parts. The first part indicates the temperature difference between the corner and the high conductivity material where the heat conduction is assumed to be flowing only in the vertical direction due to the width of the domain being larger than the height. The second part defines the temperature drop between the end of the high-conductivity material and the heat sink. Equation B-1 is derived from Fourier's heat law in appendix C-1-1.

The optimal height to length ratio is found by minimizing equation B-1. The result, derived in appendix C-1-2, is

$$\left(\frac{H_0}{L_0}\right)_{\text{opt}} = \frac{2}{\sqrt{\tilde{k}\phi_0}} < 1 \quad (\text{B-2})$$

The performance of the zeroth order construct is indicated by

$$\frac{\Delta T_0 k_0}{q''' A_0} = \frac{1}{2\sqrt{\tilde{k}\phi_0}}. \quad (\text{B-3})$$

The assumption made is that $L > H$. In equation (B-2) this occurs when the ratio between the high and low conductivity is much larger than one, $\frac{k_p}{k_0} \gg 1$, which is generally valid for flow problems. Combining equations (B-2) and (B-3) yields

$$\Delta T_{0, \min} = \frac{q''' H_0^2}{4k_0}. \quad (\text{B-4})$$

Equation (B-3) indicates that the optimal domain ratio causes the resistance through the low-conductivity material to be equal to the resistance through the high-conductivity blade. In CT, this ratio is labeled as the *equipartition principle* and supposedly exists at every scale in CT.

B-1-2 First order element

The first order construct consists of an assembly of elementary constructs. An example can be seen in figure B-2. The minimization of the temperature difference is performed in a similar manner as in the zeroth order construct. An important note is that the heat flow in the y -direction is again approximated as uniform by treating the zeroth order construct as a patch of homogeneous material with conductivity ratio $k_1 = k_p D_0 / H_0$, and thus $k_0 < k_1 < k_p$.

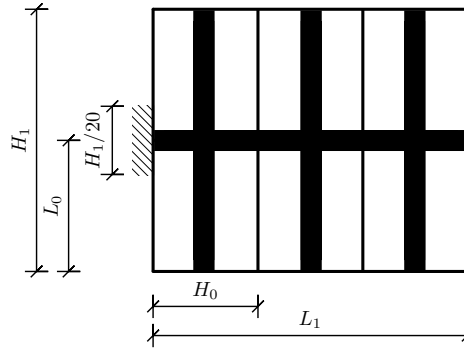


Figure B-2: Assembly of elementary designs.

By construction $H_1 = 2L_{0, \text{opt}}$ and the equation for the maximum temperature difference occurring in the design, derived in appendix C-1-3, is expressed by

$$\frac{\Delta T_1 k_1}{q''' A_1} = \frac{1}{8} \frac{H_1}{L_1} + \frac{k_1 H_1}{2k_p D_1} \frac{L_1}{H_1}. \quad (\text{B-5})$$

The derivation of the optimized shape of first order construct is more elaborate due to more design variables being present. The equations indicating the optimal shape, amount of zeroth order elements, and minimum maximum temperature are explained below.

The area of the first order construct is defined by the number n_1 of zeroth order elements through $A_1 = n_1 A_0$. The total amount of high-conductivity material is approximated, due to overlapping regions, as $A_{p,1} = D_1 L_{1, \text{opt}} + n_1 D_0 L_{0, \text{opt}}$. The amount of high-conductivity material present is $\phi_1 = A_{p,1} / A_1$. The optimal shape ratio, derived in appendix C-1-3, is

$$\left(\frac{H_1}{L_1} \right)_{\text{opt}} = 2 \left(\frac{k_1 H_1}{k_p D_1} \right)^{1/2}. \quad (\text{B-6})$$

Using this ratio, the minimum temperature is equal to

$$\frac{\Delta T_{1, \text{min}} k_1}{q''' A_1} = \frac{1}{2} \left(\frac{k_1 H_1}{k_p D_1} \right)^{1/2}. \quad (\text{B-7})$$

Using equations (B-2) the definition of k_1 and the definition of H_1 we find

$$\Delta T_{1, \min} = \frac{q''' H_0^2}{4k_0}. \quad (\text{B-8})$$

Note that this result is equal to the minimum maximum temperature in the zeroth order construct, (B-4).

Now the shape of the domain is known, the number of zeroth order constructs is optimized. The result, also derived in appendix C-1-3, is found to be

$$n_{1, \text{opt}} = 2 \frac{L_{1, \text{opt}}}{H_0} = \left(\frac{k_p D_1^2}{k_0 D_0 H_0} \right)^{1/4}. \quad (\text{B-9})$$

The final steps taken are in order to find the optimal branch thicknesses and performance of the first order construct. Through the approximation of the elementary construct as a homogeneous material and the found relation of $\Delta T_{1, \min} = \Delta T_{0, \min}$ the overall temperature difference is approximated as $\Delta T_1 = \Delta T_{0, \min} + \frac{1}{2} \Delta T_{1, \min}$. Which results in a non-dimensional thermal resistance

$$\frac{\Delta T_{1, \min} k_0}{q''' A_1} = \frac{3}{4} \left(\frac{k_0}{k_p} \right)^{3/4} \left(\frac{H_0}{D_1} \right)^{1/2} \left(\frac{H_0}{D_0} \right)^{1/4}.$$

Finally the branch width ratio is optimized and found to be

$$\left(\frac{D_1}{D_0} \right)_{\text{opt}} = \left(\frac{D_0 k_p}{H_0 k_0} \right)^{1/2} \gg 1. \quad (\text{B-10})$$

Using these values the performance of the first order construct is

$$\frac{\Delta T_1 k_0}{q''' A_1} = \frac{1}{\tilde{k} \phi_1}, \quad (\text{B-11})$$

$$\Delta T_{1, \min} = \frac{3 q''' H_0^2}{8 k_0}. \quad (\text{B-12})$$

B-1-3 Second order element

The second order construct is built up in the same way as the first order construct. The critical dimensions are found by first optimizing the aspect ratio, followed by the number of first order constructs. Finally the width of the branches is optimized. For brevity, only the performance is noted, the details can be found in Bejan (1997). The performance of the second order construct is defined by

$$\frac{\Delta T_2 k_0}{q''' A_2} = \frac{2}{\tilde{k} \phi_2}, \quad (\text{B-13})$$

$$\Delta T_{2, \min} = \frac{3}{8} \left(1 + \frac{1}{3^{1/2}} \right) \frac{q''' H_0^2}{k_0}. \quad (\text{B-14})$$

B-2 Remarks and adjustments

During the derivation of the assembly of elementary into higher order designs, the following points are of importance:

1. In the zeroth order construct $H_0 < L_0$ in order to approximate the heat flow as one dimensional. This requires the reasonable assumption that $\tilde{k} \gg 1$.
2. When assembling the first order construct, the zeroth order construct is approximated as a homogeneous material.
3. The *equipartition principle* is lost in the first order construct.

The last two points are addressed in Ghodoossi and Egrican (2003). There, the heat flow from the zeroth to the first order construct is more precisely approximated by modeling the flow from the zeroth branch to the central branch as point wise heat inputs. This leads to different domain shapes and performance values as described in the next section.

B-2-1 Adjustments to constructs

In Ghodoossi and Egrican (2003) only the dimensions of the first order construct differ from the original CT. The precise derivations can be found in appendix C-2-1. The optimal performance of the first order construct is derived as

$$\frac{\Delta T_1 k_0}{q''' A_1} = \frac{\sqrt{2}}{\tilde{k} \phi_1}. \quad (\text{B-15})$$

The performance of the second order construct is more precisely derived as

$$\frac{\Delta T_2 k_0}{q''' A_2} = \frac{9\sqrt{2}}{8\tilde{k} \phi_2}. \quad (\text{B-16})$$

In the same paper the temperature differences between the maximum and minimum occurring temperatures are derived by rewriting equations B-15. The maximum temperature in the first order construct is found to be

$$\Delta T_{1, \min} = \frac{q''' H_0^2}{2k_0}. \quad (\text{B-17})$$

Comparing the minimized maximum temperatures that occur in the zeroth and first order construct using (B-4) and (B-17) indicates a rise of a factor two. The equipartition principle thus hold only when using this more precise approximation. The maximum temperature difference in the second order construct is

$$\Delta T_2 = \frac{q''' H_0^2}{2k_0} + \frac{n_1 q''' A_0 H_1}{4k_p D_2} n_2^2.$$

When minimizing this temperature difference with respect to the number of first order constructs and ratio of branch thicknesses the result is

$$n_{2, \text{opt}} = 2\sqrt{2} \approx 2.8. \quad (\text{B-18})$$

This optimal number not being a multiple of two poses a problem: practically either two or four elements need to be placed. When the thickness of the second order element is optimized with two and four first order elements the results are

$$\frac{\Delta T_{2, \text{min}, n=2k_0}}{q''' A_2} = \frac{9\sqrt{2}}{8\tilde{k}\phi_2}, \quad (\text{B-19})$$

$$\frac{\Delta T_{2, \text{min}, n=4k_0}}{q''' A_2} = \frac{\sqrt{2}(\sqrt{2} + \sqrt{3})^2}{8\tilde{k}\phi_2}. \quad (\text{B-20})$$

Thus the better choice is placing two first order constructs in the second order construct. When now the optimal geometric features are derived using this fact and the minimized maximum temperature difference is found as $\Delta T_{2, \text{min}} = \frac{3q'''H_0^2}{4k_0}$. The minimized maximum temperature is a factor 1.5 higher than the first order construct B-17. This was expected to be a factor two as dictated by the equipartition principle. But the optimal value of n_2 could not be implemented since it needs to be an even number.

B-2-2 Closing remarks

When considering the performance of higher order constructs, (B-15) and (B-16) indicate that there is no combination of $\tilde{k}\phi$ that validates the use of the second above the first order construct Ghodoossi (2004); Kuddusi and Egrican (2008). An intuitive explanation is the fact that in the second order construct heat first flows away from the heat sink when traversing the path indicated by high conductivity material.

One of the statement in Bejan (1997) is that CT validates the existence of ‘tree-like’ shapes in nature. Why these shapes result from CT rather than the idea of minimizing of flow resistance is not clear. Furthermore, the orthogonal assembly of slender elements often resembles a three-like shape, independent of the assembly method.

These points do not obstruct the use of CT as an initial design for topology optimization. Thus, when the combination of $\tilde{k}\phi$ requires a first order design the modified design choices as suggested by Ghodoossi and Egrican (2003) are used.

Appendix C

Constructal Theory derivations

This appendix contains the derivations of the main equations describing the original and modified Constructal Theory (CT). For a description of these equations see appendix D.

C-1 Derivations of the original Constructal Theory

In this section the equations describing the original Constructal Theory are derived.

C-1-1 Heat flow in zeroth order construct

In the zeroth order construct the heat flow is approximated as two dimensional, due to the thickness of the plate being small compared to the length and height. Furthermore, the equation dictating the heat flow is approximated as a sum of two one dimensional heat flows. The first being in the y direction through the material with low conductivity k_0 . The second flow is in the x direction along the high conducting material.

The governing equation for the low conductivity heat generating material is derived from Fourier his law of thermal conduction. This law indicates that the heat flow in one direction is equal to the negative gradient of the temperature multiplied by the heat conductivity, $q'' = -k \frac{dT}{dx}$. The time dependent change in temperature of a finite volume, with heat q''' [$\frac{W}{m^3}$] being generated in the volume is

$$\frac{\partial(c_p \rho A dx T)}{\partial t} = -kA \frac{\partial T}{\partial x} \Big|_x - \left(-kA \frac{\partial T}{\partial x} \Big|_{x+dx} \right) + q''' A dx.$$

A Taylor expansion of the second to last part yields

$$-kA \frac{\partial T}{\partial x} \Big|_{x+dx} = -kA \frac{\partial T}{\partial x} \Big|_x + kA \frac{\partial^2 T}{\partial x^2} dx.$$

Substituting this in the earlier result and dividing by dx yields

$$\frac{\partial(c_p \rho A T)}{\partial t} = kA \frac{\partial^2 T}{\partial x^2} + q''' A.$$

Since c_p , ρ and A are not dependent of time these can be placed before the derivative and the equation becomes

$$c_p \rho A \frac{\partial T}{\partial t} = kA \frac{\partial^2 T}{\partial x^2} + q''' A.$$

In CT the heat flow is assumed to have reached an equilibrium the right side of the above equation is zero. Dividing by kA and reordering yields

$$\frac{\partial^2 T}{\partial x^2} + \frac{q'''}{k} = 0. \quad (\text{C-1})$$

The zeroth order construct is symmetrical around the line $y = \frac{H_0}{2}$. Only considering the top half of the plane and setting the bottom at $y = 0$ the boundary conditions are $\frac{\partial T}{\partial y} = 0$ at $y = \frac{H_0}{2}$ and $T = T_0(x)$ at $y = 0$. When implementing (C-1) for heat flow in the y direction with conductivity k_0 , integrating and implementing the first boundary condition the result is

$$\frac{\partial T}{\partial y} = \int \frac{-q'''}{k_0} dy = \frac{-q'''}{k_0} y + C_1 = \frac{-q'''}{k_0} y + \frac{q''' H_0}{2k_0}.$$

Integrating this a second time and implementing the second boundary condition yields

$$T = \int \frac{-q'''}{k_0} y + \frac{q''' H_0}{2k_0} dy = \frac{-q'''}{k_0} y^2 + \frac{q''' H_0}{2k_0} y + C_2 = \frac{q'''}{2k_0} (H_0 y - y^2) + T_0(x). \quad (\text{C-2})$$

This is the first result. To continue we need to solve the heat flow through the blade in the x direction. Applying conservation of energy with the plate having a thickness of σ yields

$$\frac{\partial(c_p \rho A dx T)}{\partial t} = -kA \frac{\partial T}{\partial x} \Big|_x - \left(-kA \frac{\partial T}{\partial x} \Big|_{x+dx} \right) + q''' H_0 dx \sigma,$$

with $A = D_0 \sigma$. Note that $q''' H_0 dx \sigma$ is the heat input on the blade from the heat generating material. The heat being generated inside the high conductivity material with area A is not considered. Using a Taylor expansion and implementing the equilibrium we find

$$\frac{\partial(c_p \rho A dx T)}{\partial t} = kD_0 \sigma dx \frac{\partial^2 T}{\partial x^2} + q''' H_0 dx \sigma = 0.$$

When dividing by σdx , the conductivity of the material being k_p , and reordering the result is

$$k_p D_0 \frac{\partial^2 T_0}{\partial x^2} + q''' H_0 = 0. \quad (\text{C-3})$$

This equation is known as the fin equation. In our application this differential equation is subject to the boundary conditions $\frac{dT_0}{dx} = 0$ at $x = L_0$ and $T_0 = T(0, 0)$ at $x = 0$. Integrating (C-3) and implementing the first boundary condition yields

$$\frac{dT_0}{dx} = - \int \frac{q''' H_0}{k_p D_0} dx = - \left(\frac{q''' H_0}{k_p D_0} \frac{x}{2} + C_1 \right) = - \frac{q''' H_0}{k_p D_0} \frac{x}{2} + \frac{q''' H_0}{k_p D_0} L_0.$$

Integrating a second time and implementing the second boundary conditions yields

$$T_0 = \int \frac{q''' H_0}{k_p D_0} (-x + L_0) dx = \frac{q''' H_0}{k_p D_0} \left(-\frac{x^2}{2} + \frac{x}{2} L_0 \right) + C_2 = \frac{q''' H_0}{k_p D_0} \left(-\frac{x^2}{2} + x L_0 \right) + T(0, 0). \quad (\text{C-4})$$

Having found the value of T_0 we substitute this in equation (C-2) which results in

$$T(x, y) - T(0, 0) = \frac{q'''}{2k_0} (H_0 y - y^2) + \frac{q''' H_0}{k_p D_0} \left(-\frac{x^2}{2} + x L_0 \right).$$

The above result indicates that the maximum temperature difference occurs at the maximum distance from the heat sink, thus at $x = L_0$ and $y = \frac{H_0}{2}$. Using these values equation B-1 is found. Note that the above relation is only valid when $y > 0$. The following assumptions and approximations have been made:

1. There is no heat being generated in the strip of high conductivity material.
2. The final equation is valid for the upper half of the design. Due to symmetry the lower half of the design has an equal temperature distribution.
3. The length of the heat path in the y direction has been approximated as $\frac{H_0}{2}$ instead of $\frac{H_0 - D_0}{2}$.

C-1-2 Optimizing the zeroth order construct

Equation B-2 is derived from equation B-1 by setting the partial derivative of B-2 to equation B-1 to zero. This indicates a stationary point. We thus solve for

$$\left(\frac{\partial \frac{\Delta T_0 k_0}{q''' A_0}}{\partial \frac{H_0}{L_0}} \right)_{\tilde{k}, \phi_0} = \frac{1}{8} - \frac{1}{2\tilde{k}\phi_0} \left(\frac{L_0}{H_0} \right)^2 = 0.$$

Using the corresponding ratio of $\frac{H_0}{L_0}$ rightfully indicates a minimum since the second derivative is a positive value,

$$\left(\frac{\partial^2 \frac{\Delta T_0 k_0}{q''' A_0}}{\partial \left(\frac{H_0}{L_0} \right)^2} \right)_{\tilde{k}, \phi_0} = \frac{1}{8} + \frac{1}{\tilde{k}\phi_0} \left(\frac{L_0}{H_0} \right)^3 > 0.$$

Solving for $\frac{L_0}{H_0}$ results in $\left(\frac{L_0}{H_0} \right)^2 = \left(\frac{\tilde{k}\phi_0}{4} \right)$. Taking the square root and inverting both sides yields B-2,

$$\left(\frac{H_0}{L_0} \right)_{\text{opt}} = \frac{2}{\sqrt{\tilde{k}\phi_0}}.$$

Now equation B-3 can easily be found by substituting the above result in B-1 as

$$\frac{\Delta T_0 k_0}{q''' A_0} = \frac{1}{8} \frac{2}{\sqrt{\tilde{k}\phi_0}} + \frac{1}{2\tilde{k}\phi_0} \frac{\sqrt{\tilde{k}\phi_0}}{2} = \frac{1}{4} \frac{1}{\sqrt{\tilde{k}\phi_0}} + \frac{1}{4\sqrt{\tilde{k}\phi_0}} = \frac{1}{2\sqrt{\tilde{k}\phi_0}}.$$

Next B-4 can be found using the above two derivations by noting that

$$\frac{1}{4} \left(\frac{H_0}{L_0} \right)_{\text{opt}} = \frac{1}{2\sqrt{\tilde{k}\phi_0}}.$$

This is equal to the right hand side of equation B-4. Substituting yields

$$\frac{\Delta T_0 k_0}{q''' A_0} = \frac{1}{4} \left(\frac{H_0}{L_0} \right).$$

Now multiplying by q''' , A_0 and dividing by k_0 yields the minimum maximum temperature in the zeroth order construct,

$$\Delta T_{0, \min} = \frac{q''' H_0^2}{4k_0}. \quad (\text{C-5})$$

C-1-3 First order construct

From equation B-5 we derive equation B-6 by again taking the partial derivative and setting this to zero,

$$\left(\frac{\partial \frac{\Delta T_1 k_1}{q''' A_1}}{\partial \frac{H_1}{L_1}} \right) = \frac{1}{8} - \frac{k_1 H_1}{2k_p D_1} \left(\frac{L_1}{H_1} \right)^2 = 0.$$

Solving for $\frac{L_1}{H_1}$ yields $\left(\frac{L_1}{H_1} \right)^2 = \left(\frac{k_p D_1}{4k_1 H_1} \right)$. Taking the square root and inverting both sides yields (B-6), indicating the optimal ratio for the first order construct

$$\left(\frac{H_1}{L_1} \right)_{\text{opt}} = 2 \left(\frac{k_1 H_1}{k_p D_1} \right)^{1/2}.$$

Implementing this result in (B-5) yields equation B-7,

$$\frac{\Delta T_1 k_1}{q''' A_1} = \frac{2}{8} \left(\frac{k_1 H_1}{k_p D_1} \right)^{1/2} + \frac{k_1 H_1}{2k_p D_1} \frac{1}{2} \left(\frac{k_p D_1}{k_1 H_1} \right)^{1/2} = \frac{1}{4} \left(\frac{k_1 H_1}{k_p D_1} \right)^{1/2}.$$

Equation B-8 is derived again using

$$\frac{1}{2} \left(\frac{k_1 H_1}{k_p D_1} \right)^{1/2} = \frac{1}{4} \left(\frac{H_1}{L_1} \right)_{\text{opt}}.$$

This being equal to the right side of equation B-7 a substitution leads to

$$\frac{\Delta T_{1, \min} k_1}{q''' A_1} = \frac{1}{4} \left(\frac{H_1}{L_1} \right)_{\text{opt}}.$$

Now multiplying by q''' , A_1 and dividing by k_1 yields

$$\Delta T_{1, \min} = \frac{q''' H_1 L_1}{k_1} \frac{1}{4} \frac{H_1}{L_1} = \frac{q''' H_1^2}{4k_1}.$$

With $k_1 = k_p \frac{D_0}{H_0}$ and $H_1 = 2L_{0, \text{opt}}$ we find $\Delta T_{1, \text{min}} = \frac{q''' L_0^2 H_0}{k_p D_0}$. Reformulating equation B-2 in order to solve for L_0 we find $L_0 = \frac{1}{2} \left(\frac{k_p D_0 H_0}{k_0} \right)^{1/2}$. By substituting this in the previous result we find

$$\Delta T_{1, \text{min}} = \frac{q''' H_0}{k_p D_0} \frac{1}{4} \left(\frac{k_p D_0 H_0}{k_0} \right) = \frac{q''' H_0^2}{k_0 \phi_0}.$$

Which is equation B-8.

Now the optimal number of zeroth order tiles in the first order element is optimized, as dictated by (B-9). To derive this we first note that $n_{1, \text{opt}}$ can be written as a function of $L_{1, \text{opt}}$ and H_0 as

$$n_{1, \text{opt}} = \frac{A_1}{A_0} = \frac{L_1 H_1}{L_0 H_0} = \frac{L_1 2L_0}{L_0 H_0} = 2 \frac{L_{1, \text{opt}}}{H_0}.$$

The right side of the equation above can be found by using the optimal $\frac{H_1}{L_1}$ and substituting previous results. First the definitions of k_1 and H_1 are substituted and the result is

$$\left(\frac{2L_0}{L_1} \right)_{\text{opt}} = 2 \left(\frac{k_p D_0 2L_0}{H_0 k_p D_1} \right)^{1/2} = 2 \left(\frac{2D_0 L_0}{H_0 D_1} \right)^{1/2}.$$

This is inverted, followed by a multiplication by $2L_0$, resulting in $L_1 = L_0 \left(\frac{H_0 D_1}{2D_0 L_0} \right)^{1/2}$. Now we divide by H_0 and substitute the optimal value of $\frac{H_0}{L_0}$ which yields

$$\frac{L_1}{H_0} = \frac{L_0}{H_0} \left(\frac{H_0 D_1}{2D_0 L_0} \right)^{1/2} = \frac{1}{2} \left(\frac{k_p D_0}{k_0 H_0} \right)^{1/2} \left(\frac{k_p D_0}{k_0 H_0} \right)^{-1/4} \left(\frac{D_1}{D_0} \right)^{1/2}.$$

Now multiplying this by 2 we reach the alternative definition of $n_{1, \text{opt}}$ as stated earlier. This definition is

$$2 \frac{L_1}{H_0} = \left(\frac{k_p D_0}{k_0 H_0} \right)^{1/4} \left(\frac{D_1}{D_0} \right)^{1/2} = \left(\frac{k_p D_1^2}{k_0 D_0 H_0} \right)^{1/4}.$$

C-2 Derivations of modified Constructal Theory

In this section the derivations leading to the equations as stated in Section B-1-1 are derived. Equations describing the zeroth order construct are not different, thus the first subsection is regarding the first order construct.

C-2-1 First order construct

Instead of approximating the heat conductivity rate of the zeroth order element as homogeneous, as Bejan does, the fin equation has been applied with heat inputs at the points where the zeroth and the first order branch meet Ghodoossi and Egrican (2003). The temperature difference between the prescribed boundary temperature and the upper or lower right corner is $\Delta T_1 = \Delta T_{M_{1n'_1} P_1} + \Delta T_{M_1 M_{1n'_1}}$. This temperature difference is composed of two terms. The temperature drop through the zeroth order blade, the first part of the equation. And the temperature drop from the source M_1 up to the point where the last zeroth order element is

in connection with the horizontal blade $M_{1n'_1}$ which is the second part of the upper equation. With $n'_1 = \frac{n_1}{2}$ the first part is known. The second part can be calculated exactly as stated below.

The temperature distribution between two points $M_{1,j-1}$ and $M_{1,j}$ is

$$\frac{d^2T}{dx^2} = 0. \quad (\text{C-6})$$

The two boundary conditions are

$$\begin{aligned} T &= T_{M_{1,j-1}} \text{ at } x = (2j-3)\frac{H_0}{2} \\ k_p D_1 \frac{dT}{dx} &= [n_1 - 2(j-1)]q''' A_0 \text{ at } x = (2j-1)\frac{H_0}{2}. \end{aligned}$$

Integrating (C-6) yields the temperature distribution between $M_{1,j-1}$ and $M_{1,j}$ as

$$T - T_{M_{1,j-1}} = \frac{[n_1 - 2(j-1)]q''' A_0}{k_p D_1} x.$$

Substituting x as stated in the second boundary condition yields

$$T_{M_{1,j}} - T_{M_{1,j-1}} = \frac{[n_1 - 2(j-1)]q''' A_0 H_0}{k_p D_1}.$$

Applying a similar procedure to the $M_1 M_{11}$ interval yields

$$T_{M_{11}} - T_{M_1} = \frac{n_1 q''' A_0 H_0}{2k_p D_1}.$$

The temperature difference along the D_1 link is equal to the sum of all temperature differences

$$\Delta T_{M_1 M_{1n'_1}} = T_{M_{11}} - T_{M_1} + \sum_{j=2}^{n'_1} (T_{M_{1,j}} - T_{M_{1,j-1}}) = \frac{n_1^2 q''' A_0 H_0}{4k_p D_1}.$$

Adding the above result to the temperature drop in the zeroth order element, equation (C-5), yields

$$\Delta T_1 = \frac{q''' H_0^2}{4k_0} + \frac{n_1^2 q''' A_0 H_0}{4k_p D_1}.$$

In order for the result to be non-dimensional, it is rewritten as

$$\frac{\Delta T_1 k_0}{q''' A_1} = \frac{1}{2n_1} \left(\frac{1}{\tilde{k}\phi_0} \right) + \frac{H_0 n_1}{4\tilde{k}D_1}. \quad (\text{C-7})$$

To reach (B-15) two steps need to be taken. First the optimal number of zeroth order constituents needs to be found. Then the optimal material allocated to the first order blade in comparison to the zeroth order blade considering the material constraint. These are performed below.

Taking the derivative of (C-7) with respect to n_1 and setting this to zero yields

$$\frac{\partial \frac{\Delta T_1 k_0}{q''' A_1}}{\partial n_1} = -\frac{1}{2n_1^2 (k\phi_0)^{1/2}} + \frac{H_0}{4D_1 k} = 0.$$

Solving for n_1 yields

$$n_1 = \left(\frac{2D_1 \tilde{k}}{H_0 (\tilde{k}\phi)^{1/2}} \right)^{1/2}.$$

Solving the earlier optimized ratio of $\left(\frac{H_0}{L_0}\right)_{\text{opt}}$ for L_0 and substituting yields $n_1 = \left(\frac{\tilde{k}D_1}{L_0}\right)^{1/2}$.

Substituting this result in equation (C-7) yields

$$\frac{\Delta T_1 k_0}{q''' A_1} = \frac{1}{2} \left(\frac{1}{\tilde{k}\phi_0} \right) \left(\frac{\tilde{k}D_1}{L_0} \right)^{-1/2} + \frac{H_0}{4\tilde{k}D_1} \left(\frac{\tilde{k}D_1}{L_0} \right)^{1/2}.$$

Solving $\left(\frac{H_0}{L_0}\right)_{\text{opt}}$ for ϕ_0 yields $\phi_0 = \left(\frac{2L_0}{H_0 \tilde{k}^{1/2}}\right)^2$. Substituting this in the previous result and reorganizing yields:

$$\frac{\Delta T_1 k_0}{q''' A_1} = \frac{1}{2\tilde{k}} \left(\frac{L_0}{D_1} \right)^{1/2} \frac{H_0 \tilde{k}^{1/2}}{2L_0} + \frac{H_0}{4} \left(\frac{1}{\tilde{k}L_0 D_1} \right)^{1/2} = \frac{H_0}{2} \left(\frac{1}{\tilde{k}L_0 D_1} \right)^{1/2} \quad (\text{C-8})$$

The optimal material distribution is now derived. The constraint on the amount of material can be written in non-dimensional form as

$$\phi_1 = \frac{A_{P_1}}{A_1} = \frac{D_1 L_1 + n_1, \text{opt} D_0 L_0}{L_1 H_1}.$$

Solving for ϕ_1 yields $D_1 = \left(\frac{n_1}{L_1}\right) (A_0 \phi_1 - D_0 L_0)$. With $L_1 = \frac{n_1 H_0}{2}$ expanding A_0 and substituting $\phi_0 = \frac{D_0}{H_0}$ we obtain

$$D_1 = \left(\frac{2}{H_0}\right) (H_0 L_0 \phi_1 - D_0 L_0) = 2L_0 \phi_1 - \frac{2D_0 L_0}{H_0} = 2L_0 (\phi_1 - \phi_0).$$

Substituting this in (C-8) and substituting the value of $\left(\frac{H_0}{L_0}\right)_{\text{opt}}$ yields

$$\frac{\Delta T_1 k_0}{q''' A_1} = \frac{H_0}{2} \left(\frac{1}{2\tilde{k}L_0^2 (\phi_1 - \phi_0)} \right)^{1/2} = \left(\frac{1}{\tilde{k}[2\phi_0 (\phi_1 - \phi_0)]^{1/2}} \right).$$

We thus need to maximize the term $[\phi_0 (\phi_1 - \phi_0)]^{1/2}$. Taking the first derivative and setting that to zero yields

$$\frac{\partial [\phi_0 (\phi_1 - \phi_0)]^{1/2}}{\partial \phi_1} = \frac{1}{2} \left(\frac{\phi_1}{\phi_0} \right)^{1/2} - 1 = 0.$$

Solving for ϕ_1 indicates $\phi_1 = 2\phi_0$. By substituting this optimal value in the original result we obtain

$$\frac{\Delta T_1 k_0}{q''' A_1} = \frac{\sqrt{2}}{\tilde{k}\phi_1}.$$

Which is equation (B-15).

Appendix D

Area to point flow through the dislodging of elements

In Errera and Bejan (1998); Bejan (2007) Constructal Theory is applied to simulate the forming of river drainage basins. In nature, river basins are formed due to water dislodging and carrying away solid particles. This is simulated by starting with a discretized field of material with a low permeability and removing elements once a pressure drop over the element is present. A detailed description follows.

The model domain consists of a fixed volume with width W , length L , and height H , where $H \ll W, L$. A certain mass flow per unit area $\dot{m}'' [\frac{\text{kg}}{\text{m}^2\text{s}}]$ in exists on the WL plane, which for brevity will be noted as \dot{m} . Except for a small opening, all the boundaries of the volume are impermeable. Due to the pressure field $P(x, y)$, the fluid is driven to the outlet. The domain is visible in figure D-1a.

The volume is discretized into square elements with a size of D^2H and a permeability of $K_{\text{low}} [\text{m}^2]$. The flow through this medium is modeled using Darcy his law. This law describes the flow of fluid through a porous medium and is applicable to viscous, laminar flow. With a fluid viscosity of $\mu [\frac{\text{kg}}{\text{ms}}]$ the volume-average velocity component in the x direction is $u = -\frac{K}{\mu} \frac{\partial P}{\partial x}$ and in the y direction it is $v = -\frac{K}{\mu} \frac{\partial P}{\partial y}$. Using these equations and the conservation of mass the pressure field is described as

$$\frac{\partial^2 P}{\partial x^2} + \frac{\partial^2 P}{\partial y^2} + \frac{\dot{m}\nu}{HK} = 0, \quad (\text{D-1})$$

with $\nu = \frac{\mu}{\rho}$ being the kinematic viscosity. The objective is the minimization of the ratio between the maximum pressure P_{peak} and the total flow rate $\dot{m}WL$. The objective improves due to the dislodging and removing of elements. This occurs when the yield shear stress, as averaged over an element base, D^2 , exceeds τ . With \mathbf{s} being the direction of the resultant of all pressure forces on the block perimeter, a block is dislodges when

$$\left(\frac{\partial P}{\partial \mathbf{s}} \right) H > \tau. \quad (\text{D-2})$$

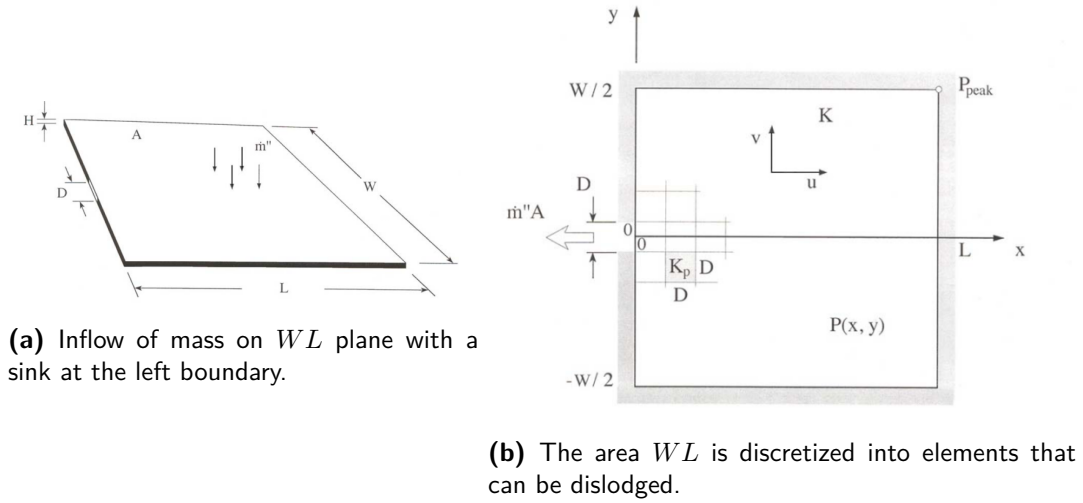
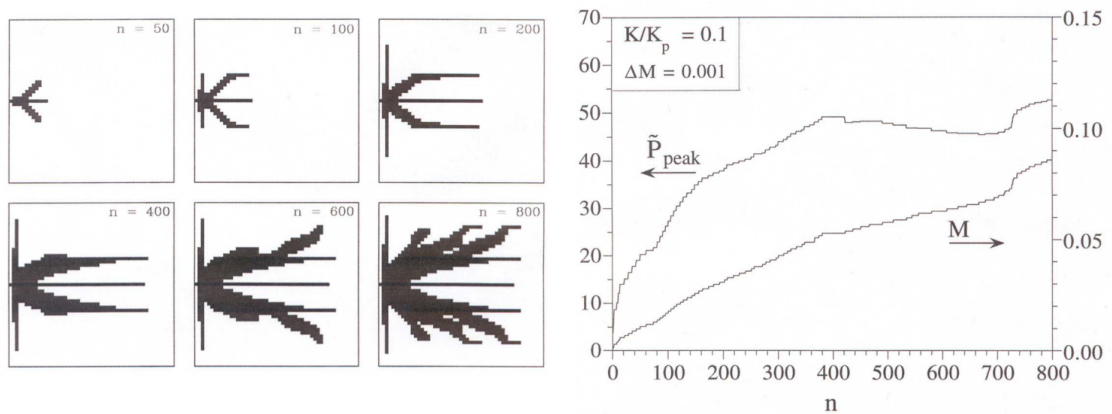


Figure D-1: Drainage basin design domain. Both figures are copied from Bejan (2007).

When a block is removed, the resulting volume is assigned a higher permeability K_{high} . Starting with all elements having a permeability of K_{low} , \dot{m} is slowly increased, (D-2) is calculated for all elements and the permeability of dislodged elements is replaced by K_{high} . If an element is dislodged, the pressure field is recalculated and (D-2) is checked again for all elements. This is repeated until no elements are dislodged, after which \dot{m} is slightly increased. Figure D-2a displays the resulting drainage basins after removing an n amount of elements with the mesh originally containing 2601 elements. The value of the non-dimensional objective function $\tilde{P} = \frac{P_{max}}{\tau D/H}$ is plotted alongside the dimensionless flow $M = \frac{\dot{m} \nu D}{\tau K}$ in figure D-2b.



(a) Emerging shapes after the removal of n elements. **(b)** The shift of the peak pressure as the flow rate is increased.

Figure D-2: Resulting drainage-basin designs and objective trends when increasing the mass input. Both figures are copied from Bejan (2007).

The shapes obtained in river drainage basin designs are clearly more complex than the assemblies of elementary designs (see appendix). Mapping the river-drainage-basin solution to a configuration of a heat problem will probably result in a design with a higher performance

than this assembly. The two methods have not been quantitatively compared. This is due to the design having more freedom and it being modified according to local gradient-information rather than a global objective function. Unfortunately the generation of these designs is expensive due to every calculation of the pressure field requiring a FEM solve. Thus dislodging n elements can result in the requirement of n solves of a system of linear equations. The size of the system can be reduced by exploiting the symmetry.

Appendix E

Problem library performance profiles

This appendix contains a large amount of performance profiles. These include figures that indicate the performance of different IDs for a single performance, the aggregated performance of all IDs, and the performance of MMA when not penalized. The profiles are ordered according to the different problems optimized.

Minimum mechanical compliance

Figure E-1 indicates each optimizer specific performance when considering the different IDs for the mechanical compliance problems.

Thermodynamic compliance

Figure E-2 indicates the performance of the unique IDs while Figure E-3 shows the optimizer specific performance when considering the different IDs for the thermodynamic compliance problems.

Minimum volume, mechanical

Figure E-4 shows the performance of IPOPT for the mechanical minimum volume problems. Due to MMA being heavily penalized, the performance profiles contain little information and are not shown here.

Minimum volume, thermodynamic

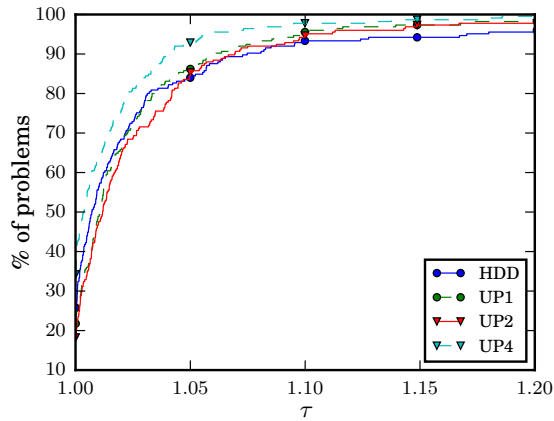
Figure E-4 shows the performance of IPOPT for the thermodynamic minimum volume problems. Due to MMA being heavily penalized, the performance profiles contain little information and are not shown here.

Compliant mechanism design

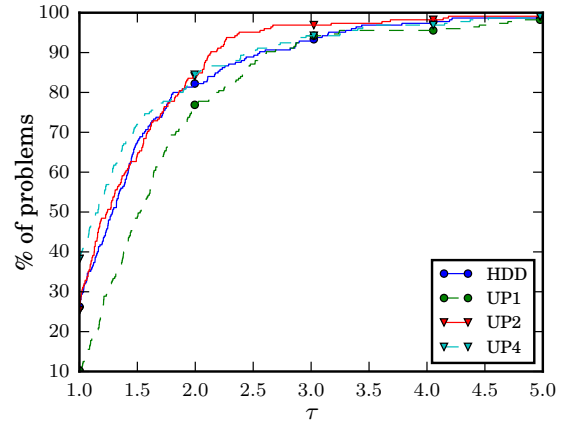
Figure E-6 shows the optimizer specific performance when considering the different IDs for the compliant mechanism design problems.

MMA when not penalized

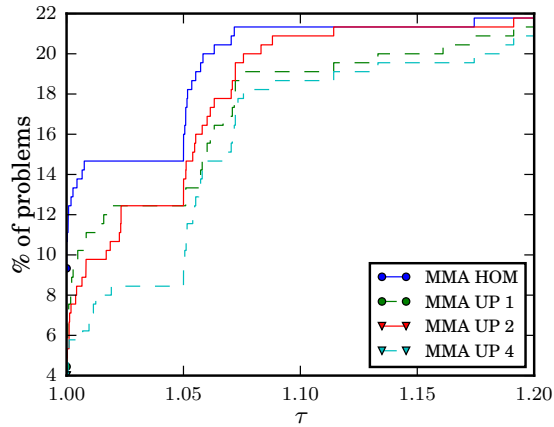
Figure E-7 shows the performance profiles of MMA regarding the objective function value for different problems when not applying penalization.



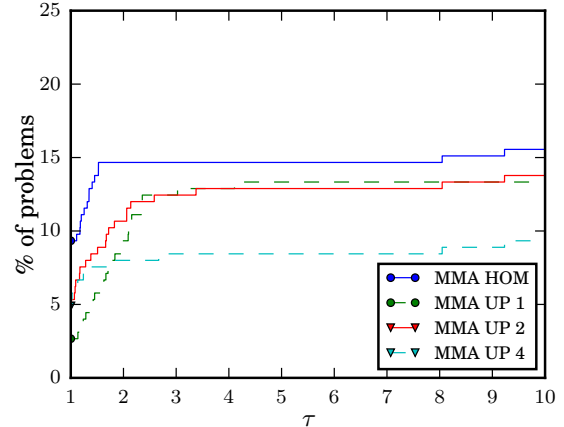
(a) Objective function value of IPOPT



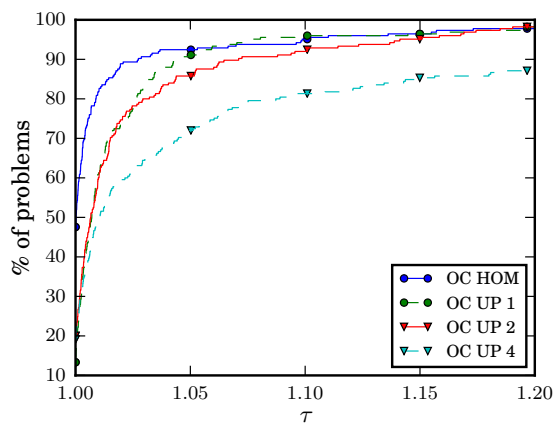
(b) Solves of IPOPT



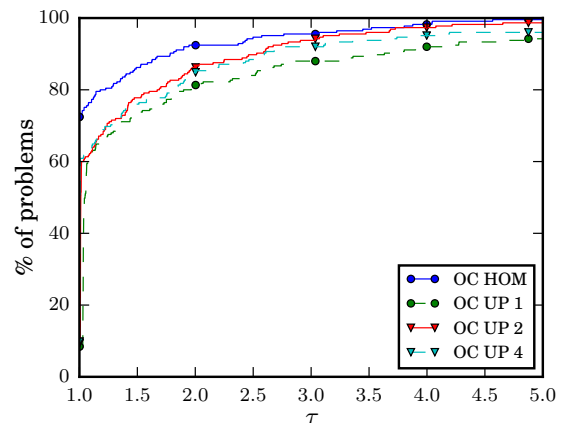
(c) Objective function value of MMA



(d) Solves of MMA



(e) Objective function value of OC



(f) Solves of OC

Figure E-1: Performance profiles of each solver with all tested initial designs for the 225 minimum mechanical compliance problems.

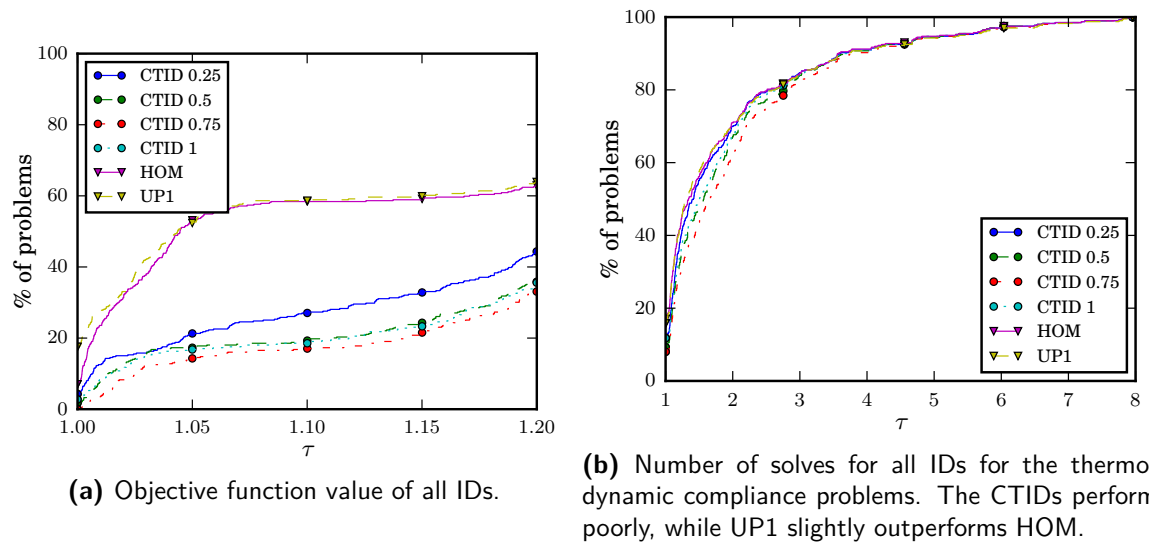
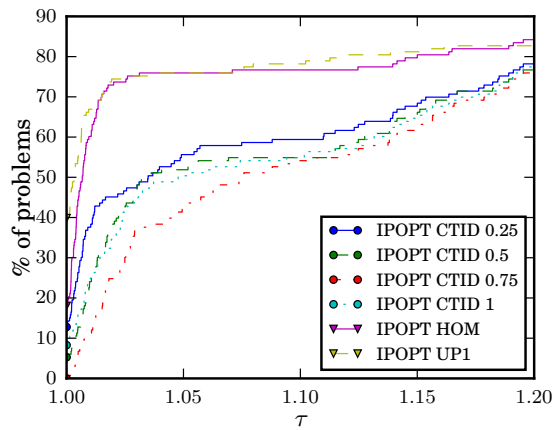
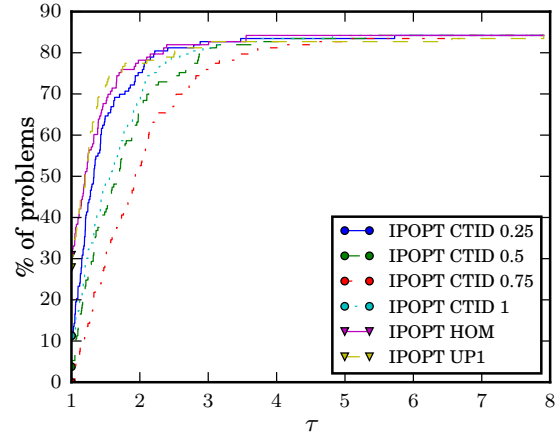


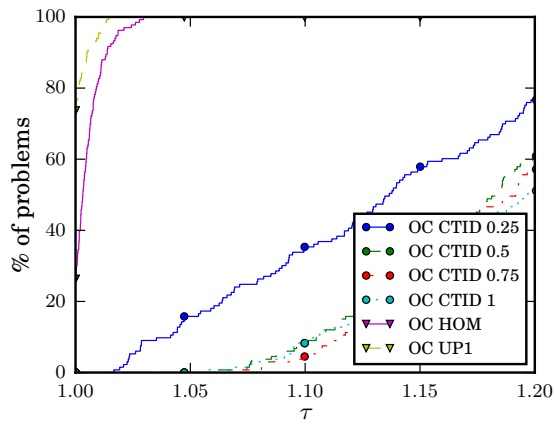
Figure E-2: Aggregating the optimizers indicates the performance of the IDs independent of the optimizers.



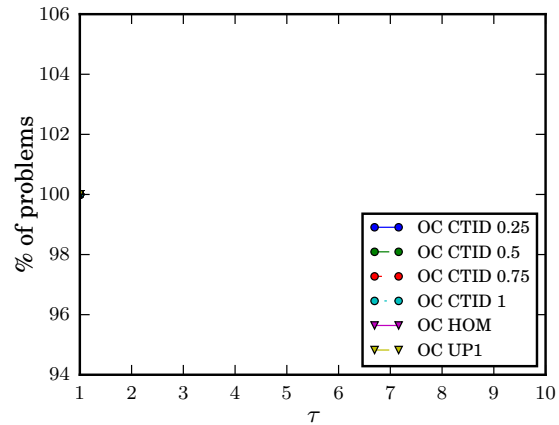
(a) Objective function value of IPOPT.



(b) Solves of IPOPT.

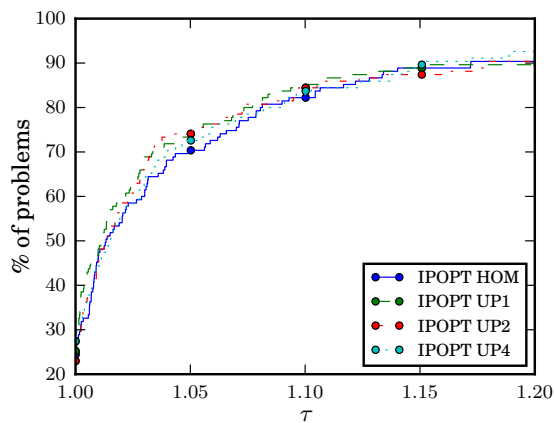


(c) Objective function value of OC.

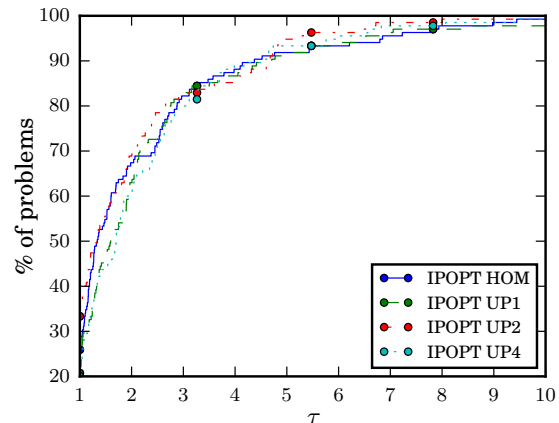


(d) Solves of OC.

Figure E-3: Solver specific performance when optimizing the thermodynamic compliance problems. The number of solves of OC indicate all IDs requiring an equal amount of solves, the profile do not differ. As this is also the case for MMA, the profiles are not shown here.



(a) Objective function value of IPOPT.



(b) Number of solves of IPOPT.

Figure E-4: Performance of IPOPT when optimizing the mechanical minimum volume problems.

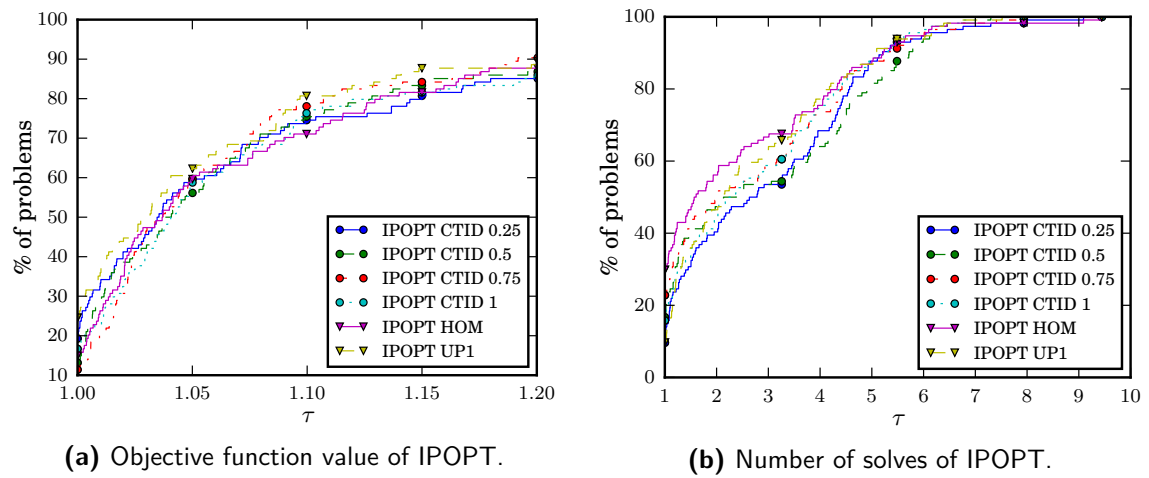
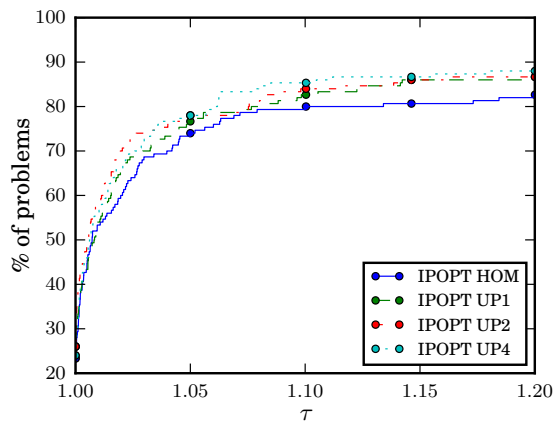
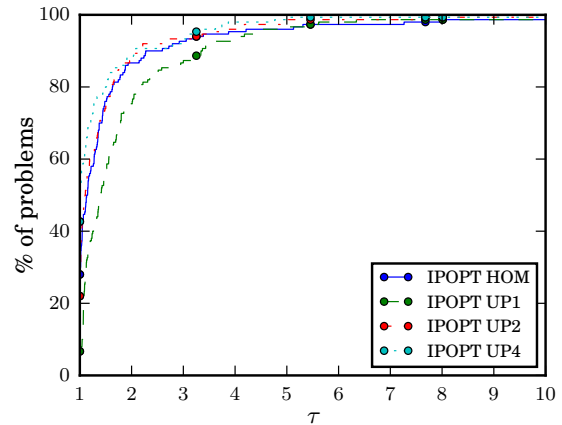


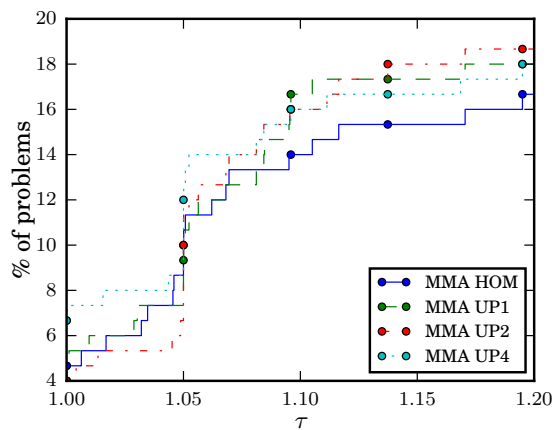
Figure E-5: Performance of IPOPT when optimizing the thermodynamic minimum volume problems.



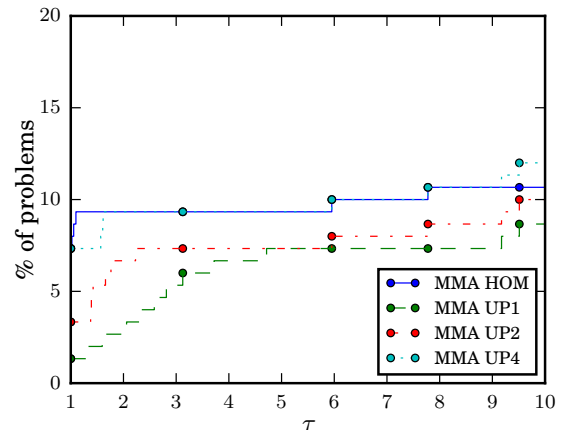
(a) Objective function value of IPOPT



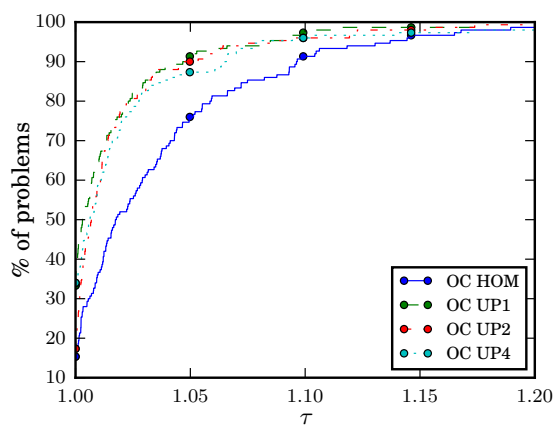
(b) Solves of IPOPT



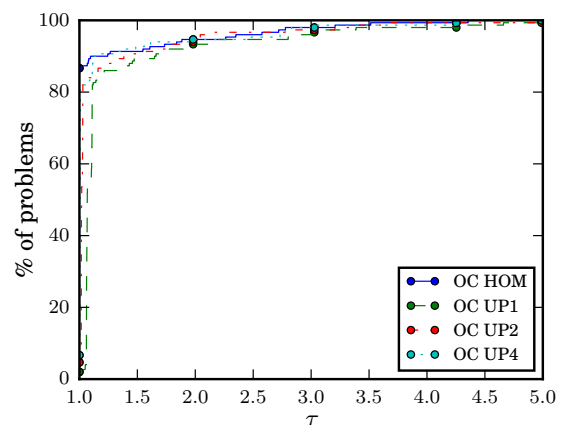
(c) Objective function value of MMA



(d) Solves of MMA

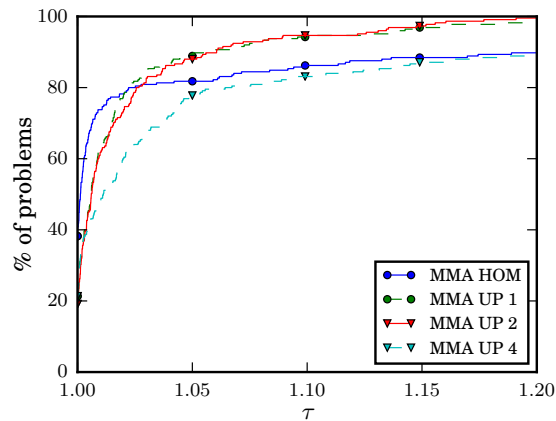


(e) Objective function value of OC

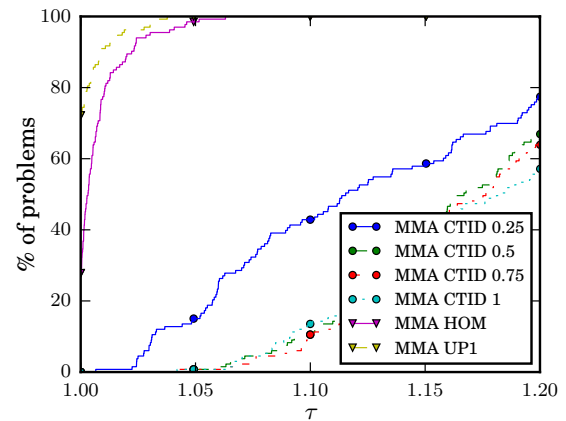


(f) Solves of OC

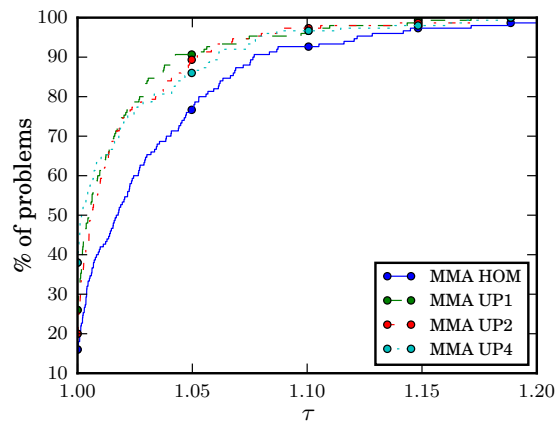
Figure E-6: Performance profiles of each solver with all tested initial designs for the 150 compliant mechanism problems.



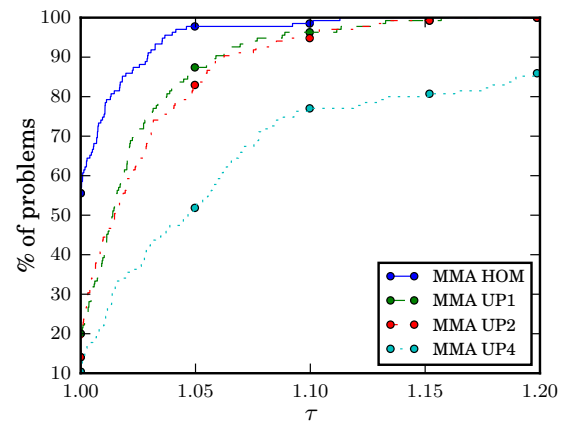
(a) Objective function value of MMA for the 225 mechanical compliance problems.



(b) Objective function value of MMA for the 133 thermodynamic compliance problems.



(c) Objective function value of MMA for the 150 compliant mechanism design problems.



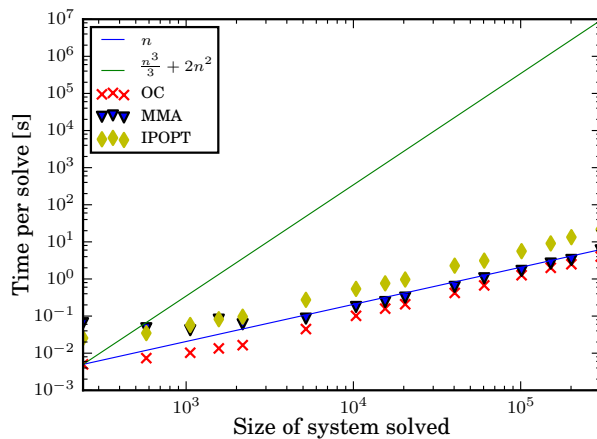
(d) Objective function value of MMA for the 135 minimum volume mechanical compliance problems.

Figure E-7: Performance profiles of MMA optimizer when not penalizing inaccurate designs. MMA UP generally outperforms MMA HOM. A clear exception is the minimum volume problem.

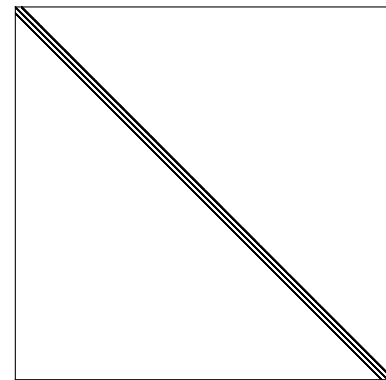
Appendix F

Computational cost of different mesh sizes

The approximate solution to the unpenalized problem is solved on different mesh sizes. In order to estimate the computation cost of a solve on each mesh size, an experiment is performed. This consists of optimizing a minimum mechanical compliance MBB problem using constant parameters and dimension ratios, but a varying amount of elements. The problem is optimized for 15 different mesh sizes, containing between 100 and 150,000 finite elements. The computation time per solve is noted for each problem and is visible in Figure F-1a. The relation between the size of the system solved and the required time scales according to the number of degrees of freedom, n . This is less than the theoretical value of $(\frac{n^3}{3}) + 2n^2$, the first part representing the *Cholesky* factorization and the second part the forward and backward factorization of the upper and lower triangular matrices. This might be due to the matrices being very sparse, as visible for one case in Figure F-1b. Using these empirical results an approximate UP2, combining four elements, is assigned a computation time factor of approximately $\frac{1}{4}$ of the original mesh size while UP4, combining sixteen elements is assigned a time factor of approximately $\frac{1}{16}$.



(a) The growth in computation time is less than expected.



(b) Sparse matrix of MBB problem containing 3600 finite elements.

Figure F-1: System solving times and image indicating matrix sparsity.

Bibliography

- G Allaire and R V Kohn. *Topology Optimization and Optimal Shape Design Using Homogenization*, pages 207–218. Springer Netherlands, Dordrecht, 1993. ISBN 978-94-011-1804-0. doi: 10.1007/978-94-011-1804-0_14. URL http://dx.doi.org/10.1007/978-94-011-1804-0_{_}14.
- Casper Schousboe Andreasen, Allan Roulund Gersborg, and Ole Sigmund. Topology optimization of microfluidic mixers. *International Journal for Numerical Methods in Fluids*, 61:498–513, 2009. URL <http://dx.doi.org/10.1002/flid.1964>.
- Erik Andreassen, Anders Clausen, Mattias Schevenels, Boyan S. Lazarov, and Ole Sigmund. Efficient topology optimization in MATLAB using 88 lines of code. *Structural and Multidisciplinary Optimization*, 43(1):1–16, 2011. ISSN 1615147X. doi: 10.1007/s00158-010-0594-7.
- T Bäck. *Evolutionary Algorithms in Theory and Practice: Evolution Strategies, Evolutionary Programming, Genetic Algorithms*. Oxford University Press, 1996.
- M. Beekers. Topology optimization using a dual method with discrete variables. *Structural Optimization*, 17(1):14–24, 1999. ISSN 0934-4373. doi: 10.1007/BF01197709.
- A. Bejan. Constructal theory of pattern formation. *Hydrology and Earth System Sciences*, 11(2):753–768, 2007. ISSN 18122116. doi: 10.5194/hess-11-753-2007. URL <http://www.hydrol-earth-syst-sci.net/11/753/2007/>.
- Adrian Bejan. Constructal-theory network of conducting paths for cooling a heat generating volume. *International Journal of Heat and Mass Transfer*, 40(4):799–816, 1997. ISSN 00179310. doi: 10.1016/0017-9310(96)00175-5.
- Adrian Bejan. *Shape and Structure, from Engineering to Nature*, 2001.
- Adrian Bejan and Marcelo R. Errera. Deterministic Tree Networks for Fluid Flow: Geometry for Minimal Flow Resistance Between a Volume and One Point. *Fractals*, 5(4), 1997.
- Adrian Bejan, George Tsatsaronis, and Michael Moran. *Thermal Design and Optimization*. Wiley, 1995. ISBN 978-0-471-58467-4.

- M P Bendsøe. Optimal shape design as a material distribution problem. *Structural optimization*, 1(4):193–202, 1989. ISSN 1615-1488. doi: 10.1007/BF01650949. URL <http://dx.doi.org/10.1007/BF01650949>.
- M P Bendsøe and O. Sigmund. *Topology optimization: theory, methods, and applications*. Number 724. 2nd edition, 2003. ISBN 3540429921. doi: 10.1063/1.3278595.
- Martin Philip Bendsøe and Noboru Kikuchi. Generating optimal topologies in structural design using a homogenization method. *Computer methods in applied mechanics and engineering*, 71:197–224, 1988.
- M.P Bendsøe and O. Sigmund. *Topology Optimization*. Number 9. 2003. ISBN 9788578110796. doi: 10.1017/CBO9781107415324.004.
- Hande Y Benson, David F Shanno, and Robert J Vanderbei. *A Comparative Study of Large-Scale Nonlinear Optimization Algorithms*, pages 95–127. Springer US, Boston, MA, 2003. ISBN 978-1-4613-0241-4.
- P.T. Boggs and J.W. Tolle. Sequential quadratic programming. *Acta Numerica*, (4):1–51, 1995.
- Blaise Bourdin. Filters in topology optimization. *International Journal for Numerical Methods in Engineering*, 50(9):2143–2158, 2001. ISSN 1097-0207. doi: 10.1002/nme.116. URL <http://https://doi.org/10.1002/nme.116>.
- Mark Christian, E Manuel, and Po Ting. International Journal of Heat and Mass Transfer Design explorations of heat conductive pathways. *International Journal of Heat and Mass Transfer*, 104:835–851, 2016. ISSN 0017-9310. doi: 10.1016/j.ijheatmasstransfer.2016.08.077.
- Elizabeth D. Dolan and Jorge J. Moré. Benchmarking optimization software with performance profiles. *Mathematical Programming, Series B*, 91(2):201–213, 2002. ISSN 00255610. doi: 10.1007/s101070100263.
- M R Errera and A Bejan. Deterministic Tree Networks for River Drainage Basins. *Fractals*, 06(03):245–261, 1998. doi: 10.1142/S0218348X98000298.
- C Fleury. CONLIN: An efficient dual optimizer based on convex approximation concepts. *Structural optimization*, 1(2):81–89, jun 1989. ISSN 1615-1488. doi: 10.1007/BF01637664. URL <http://dx.doi.org/10.1007/BF01637664>.
- A. Forsgren. On warm starts for interior methods. *System Modeling and Optimization: Proceedings of the 22nd IFIP TC7 Conference held from July 18–22, 2005, in Turin, Italy*, year="2006, 199, 2006.
- Michael R Garey and David S Johnson. *Computers and Intractability; A Guide to the Theory of NP-Completeness*. W. H. Freeman & Co., New York, NY, USA, 1990. ISBN 0716710455.
- Lotfollah Ghodoossi. Conceptual study on constructal theory. *Energy Conversion and Management*, 45(9-10):1379–1395, 2004. ISSN 01968904. doi: 10.1016/j.enconman.2003.09.002.

- Lotfollah Ghodoossi and Nilufer Egrican. Exact solution for cooling of electronics using constructal theory. *Journal of Applied Physics*, 93(8):4922, 2003. ISSN 00218979. doi: 10.1063/1.1562008.
- R. Horst and Hoang Tuy. *Global Optimization*. Springer, 1995.
- Lutfullah Kuddusi and Nilufer Egrican. A critical review of constructal theory. *Energy Conversion and Management*, 49(5):1283–1294, 2008. ISSN 01968904. doi: 10.1016/j.enconman.2007.05.023.
- G.K. K Lau, H. Du, and M.K. K Lim. Convex analysis for topology optimization of compliant mechanisms. *Structural and Multidisciplinary Optimization*, 22(4):284–294, 2001. ISSN 1615-147X. doi: 10.1007/PL00013283. URL <http://link.springer.com/10.1007/PL00013283>.
- Danny J Lohan, Ercan M Dede, and James T Allison. Topology Optimization for Heat Conduction Using Generative Design Algorithms. (June):2–7, 2015.
- Jr. Nelson R. A. and A Bejan. Constructal Optimization of Internal Flow Geometry in Convection. *Journal of Heat Transfer*, 120(2):357–364, may 1998. ISSN 0022-1481. URL <http://dx.doi.org/10.1115/1.2824257>.
- Joakim Petersson. A Finite Element Analysis of Optimal Variable Thickness Sheets. *SIAM J. Numer. Anal.*, 36(6):1759–1778, 1999. ISSN 0036-1429. doi: 10.1137/S0036142996313968. URL <http://dx.doi.org/10.1137/S0036142996313968>.
- M. H. Rasmussen and M. Stolpe. Global optimization of discrete truss topology design problems using a parallel cut-and-branch method. *Computers and Structures*, 86(13-14):1527–1538, 2008. ISSN 00457949. doi: 10.1016/j.compstruc.2007.05.019.
- Susana Rojas-Labanda and M. Stolpe. Benchmarking optimization solvers for structural topology optimization. *Structural and Multidisciplinary Optimization*, 52(3):527–547, 2015a. ISSN 16151488. doi: 10.1007/s00158-015-1250-z.
- Susana Rojas-Labanda and Mathias Stolpe. Automatic penalty continuation in structural topology optimization. *Structural and Multidisciplinary Optimization*, 52(6):1205–1221, 2015b. ISSN 16151488. doi: 10.1007/s00158-015-1277-1.
- G. I N Rozvany. A critical review of established methods of structural topology optimization. *Structural and Multidisciplinary Optimization*, 37(3):217–237, 2009. ISSN 1615147X. doi: 10.1007/s00158-007-0217-0.
- G. I N Rozvany and M. Zhou. The COC algorithm, part I: Cross-section optimization or sizing. *Computer Methods in Applied Mechanics and Engineering*, 89(1-3):281–308, 1991. ISSN 00457825. doi: 10.1016/0045-7825(91)90045-8.
- Hamid Salimi. Stochastic Fractal Search: A powerful metaheuristic algorithm. *Knowledge-Based Systems*, 75:1–18, 2015. ISSN 0950-7051. doi: <http://doi.org/10.1016/j.knosys.2014.07.025>.

- O. Sigmund. Design of multiphysics actuators using topology optimization - Part I: One-material structures. *Computer Methods in Applied Mechanics and Engineering*, 190(49-50): 6577–6604, 2001a.
- O. Sigmund. Design of multiphysics actuators using topology optimization - Part II: Two-material structures. *Computer Methods in Applied Mechanics and Engineering*, 190(49-50): 6605–6627, 2001b. ISSN 00457825. doi: 10.1016/S0045-7825(01)00252-3.
- O. Sigmund and J. Petersson. Numerical instabilities in topology optimization: A survey on procedures dealing with checkerboards, mesh-dependencies and local minima. *Structural Optimization*, 16(1):68–75, 1998. ISSN 0934-4373. doi: 10.1007/BF01214002.
- Ole Sigmund. On the usefulness of non-gradient approaches in topology optimization. *Structural and Multidisciplinary Optimization*, 43(5):589–596, 2011. doi: 10.1007/s00158-011-0638-7.
- Ole Sigmund and Kurt Maute. Topology optimization approaches A comparative review. pages 1031–1055, 2013. doi: 10.1007/s00158-013-0978-6.
- M. Stolpe. On some fundamental properties of structural topology optimization problems. *Structural and Multidisciplinary Optimization*, 41(5):661–670, 2010. ISSN 1615147X. doi: 10.1007/s00158-009-0476-z.
- M. Stolpe and K. Svanberg. On the trajectories of penalization methods for topology optimization. *Structural and Multidisciplinary Optimization*, 21(2):128–139, 2001. ISSN 1615147X. doi: 10.1007/s001580050177.
- M. Stolpe and K Svanberg. Modelling topology optimization problems as linear mixed 0–1 programs. 739(September 2002):723–739, 2003. doi: 10.1002/nme.700.
- Krister Svanberg. The method of moving asymptotes – a new method for structural optimization. *International Journal for Numerical Methods in Engineering*, 24(2):359–373, 1987. ISSN 1097-0207. doi: 10.1002/nme.1620240207. URL <http://dx.doi.org/10.1002/nme.1620240207>.
- Krister Svanberg. A class of globally convergent optimization methods based on conservative convex separable approximations. *SIAM Journal on Optimization*, pages 555–573, 2002.
- a Tovar and Kapil Khandelwal. Uniqueness in linear and nonlinear topology optimization and approximate solutions. *2nd International Conference on Engineering Optimization*, pages 1–10, 2010.
- Andrés Tovar and Kapil Khandelwal. Continuation method and filter reduction in global topology optimization. (May):2–3, 2011. URL <http://www.cmm.il.pw.edu.pl/cd/pdf/228.pdf>.
- N.P. van Dijk, M. Langelaar, and F. van Keulen. Critical Study of Design Parametrization in Topology Optimization: the influence of design parametrization on local minima. *2nd International Conference on Engineering Optimization*, pages 1–11, 2010.

- Alexander Verbart, Nico Van Dijk, Laura Del Tin, Matthijs Langelaar, and Fred van Keulen. Effect of design parameterization and relaxation on model responses in topology optimization with stress constraints. pages 1–14, 2011.
- Andreas Wächter and Lorenz T. Biegler. On the Implementation of Primal-Dual Interior Point Filter Line Search Algorithm for Large-Scale Nonlinear Programming. *Mathematical Programming*, 106(1):25–57, 2006. ISSN 0025-5610. doi: 10.1007/s10107-004-0559-y.
- W Wenzel and K Hamacher. Stochastic Tunneling Approach for Global Minimization of Complex Potential Energy Landscapes. *Phys. Rev. Lett.*, 82(15):3003–3007, apr 1999. doi: 10.1103/PhysRevLett.82.3003.
- D. F. Yates, A. B. Templeman, and T. B. Boffey. The complexity of procedures for determining minimum weight trusses with discrete member sizes. *International Journal of Solids and Structures*, 18(6):487–495, 1982. ISSN 00207683. doi: 10.1016/0020-7683(82)90065-8.
- M. Zhou and G. I N Rozvany. The COC algorithm, Part II: Topological, geometrical and generalized shape optimization. *Computer Methods in Applied Mechanics and Engineering*, 89(1-3):309–336, 1991. ISSN 00457825. doi: 10.1016/0045-7825(91)90046-9.

